Published online 13 May 2017

Nucleic Acids Research, 2017, Vol. 45, No. 12 ***7455–7473***
doi: 10.1093/nar/gkx424

Implication of the box C/D snoRNP assembly factor Rsa1p in U3 snoRNP assembly

Benjamin Rothé, Xavier Manival, Nicolas Rolland, Christophe Charron, Véronique Senty-Ségault, Christiane Branlant and Bruno Charpentier*

Ingénierie Moléculaire et Physiopathologie Articulaire (IMoPA), UMR 7365 CNRS Université de Lorraine, Biopôle, Campus Biologie Santé, 9 avenue de la forêt de Haye, BP 20199, 54505 Vandœuvre-lès-Nancy, France

Received December 08, 2016; Revised April 26, 2017; Editorial Decision April 28, 2017; Accepted May 02, 2017

ABSTRACT

The U3 box C/D snoRNA is one key element of 90S pre-ribosome. It contains a 5′ domain pairing with pre-rRNA and the $U3_{B/C}$ and $U3_{C'/D}$ motifs for U3 packaging into a unique small nucleolar ribonucleoprotein particle (snoRNP). The RNA-binding protein Snu13/SNU13 nucleates on $U3_{B/C}$ the assembly of box C/D proteins Nop1p/FBL and Nop56p/NOP56, and the U3-specific protein Rrp9p/U3-55K. Snu13p/SNU13 has a much lower affinity for $U3_{C'/D}$ but nevertheless forms on this motif an RNP with box C/D proteins Nop1p/FBL and Nop58p/NOP58. In this study, we characterized the influence of the RNP assembly protein Rsa1 in the early steps of U3 snoRNP biogenesis in yeast and we propose a refined model of U3 snoRNP biogenesis. While recombinant Snu13p enhances the binding of Rrp9p to $U3_{B/C}$, we observed that Rsa1p has no effect on this activity but forms with Snu13p and Rrp9p a $U3_{B/C}$ pre-RNP. In contrast, we found that Rsa1p enhances Snu13p binding on $U3_{C'/D}$. RNA footprinting experiments indicate that this positive effect most likely occurs by direct contacts of Rsa1p with the U3 snoRNA 5′ domain. In light of the recent U3 snoRNP cryo-EM structures, our data suggest that Rsa1p has a dual role by also preventing formation of a premature functional U3 RNP.

INTRODUCTION

In eukaryotes, ribosome biosynthesis is initiated by transcription of a pre-ribosomal RNA (pre-rRNA) 35S/45S (yeast/human cells) by RNA polymerase I. This precursor is chemically modified and processed through a series of ordered endo- and exo-ribonucleolytic cleavages to generate mature 18S, 5.8S and 25S/28S rRNAs (for review, (1,2)). These nucleolar processes involve a great number of *trans*-acting factors (for review, (3)), among which hundreds of box H/ACA and C/D small nucleolar ribonucleoprotein particles (snoRNPs) are catalysts of rRNAs pseudouridylation and ribose 2′-*O*-methylation, respectively (for review, (4,5)). In addition, a subset of snoRNPs, including U3, U14, U8 and snR30/U17, are required for endo-ribonucleolytic cleavages in the pre-rRNA (for review, (4,5)).

Box C/D snoRNAs contain two conserved sequences, namely box C (5′-RUGAUGA-3′, where R is a purine) and box D (5′-CUGA-3′), which are respectively located close to the 5′ and 3′ ends of the RNA (6). A second related couple of boxes C′ and D′ can also be present (7,8). Box C/D RNAs with a 2′-O methylation guiding activity, contain one or two guide sequences flanking box D or both boxes D and D′. They base-pair with a target sequence to specify the site to modify (7,8). Boxes C and D combine to form a box C/D RNA motif (9), folded into a kink-turn (K-turn) structure. This widespread RNA structural motif consists of two helices (I and II) surrounding a 3-nt bulge (10,11) (Figure 1A and B). Helix II is primed by two sheared G:A base pairs that are followed by a highly conserved U•U base pair in C/D box motifs (9). The box C/D snoRNAs K-turn motif constitutes a specific binding site for Snu13p/SNU13 (alias 15.5K) that nucleates RNP formation through the subsequent recruitment of Nop58p/NOP58 and the SAM-dependent 2′-*O*-methylase Nop1p/FBL (9,12) (*NB*. for clarity, separation of two protein names by the slash symbol refers to the yeast protein name followed by its human counterpart). This half-particle clamps the snoRNA at both extremities and has a major contribution for snoRNA stability (13). The internal C′ and D′ boxes form a C′/D′ motif folded into a K-turn structure or a K-loop in which helix I is replaced by a loop. The C′/D′ motif constitutes a secondary Snu13p/SNU13 binding site and the Snu13p/SNU13–C′/D′ snoRNA complex nucleates the assembly of a second half-particle through

*To whom correspondence should be addressed. Tel: +33 3 72 74 66 27; Fax: +33 3 72 74 65 45; Email bruno.charpentier@univ-lorraine.fr
Present addresses:
Benjamin Rothé, Ecole polytechnique fédérale de Lausanne (EPFL) SV ISREC, Station 19, CH-1015 Lausanne, Switzerland.
Véronique Senty-Ségault, Protein Science Facility, SFR BioSciences, Institut de Biologie et Chimie des Protéines, 7, passage du Vercors, 69367 Lyon Cedex 7, France.

© The Author(s) 2017. Published by Oxford University Press on behalf of Nucleic Acids Research.
This is an Open Access article distributed under the terms of the Creative Commons Attribution License (http://creativecommons.org/licenses/by-nc/4.0/), which permits non-commercial re-use, distribution, and reproduction in any medium, provided the original work is properly cited. For commercial re-use, please contact journals.permissions@oup.com

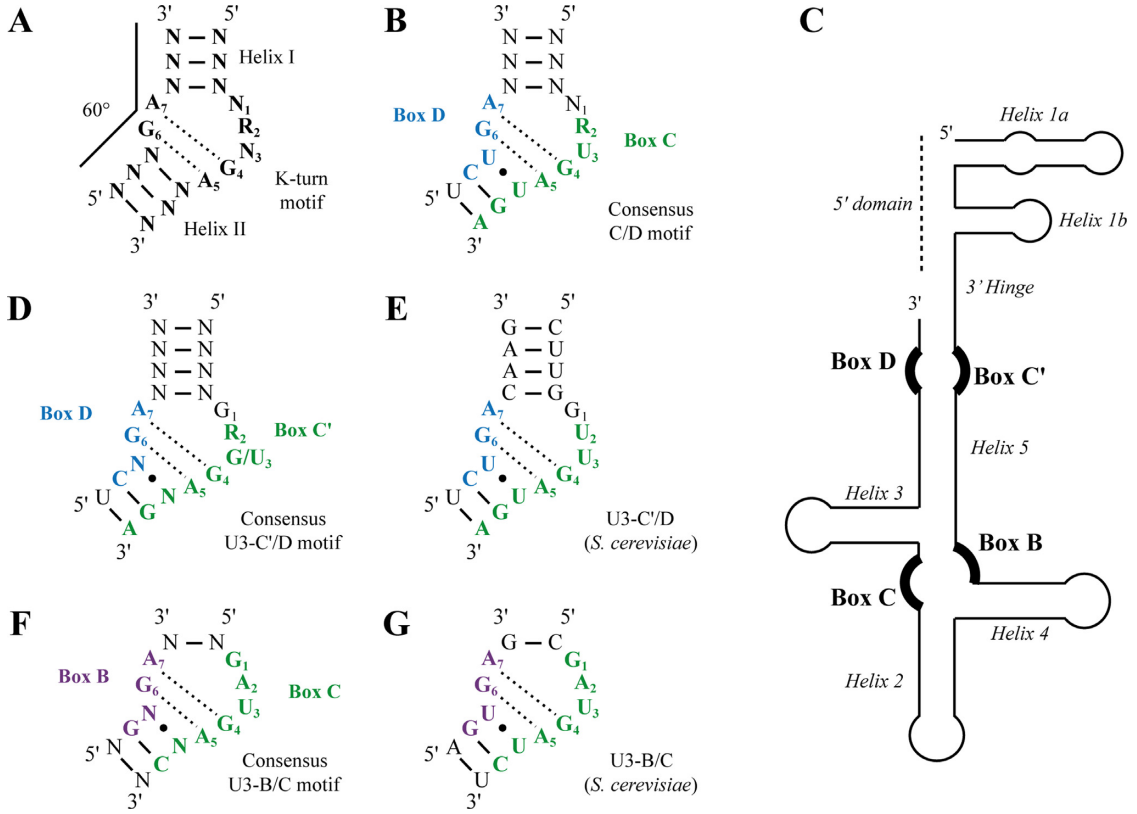

Figure 1. Overview of K-turn motifs found in the box C/D snoRNA family. (**A**) Schematic representation of a K-turn motif. Helices I and II are displayed. The sheared G:A base pairs are indicated by dotted lines. (**B**) Schematic representation of a consensus box C/D motif. (**C**) Schematic representation of the yeast U3 snoRNA. The 3′ part of the molecule contains two K-turn motifs, namely $U3_{C'/D}$ and $U3_{B/C}$ motifs. The 5′ functional domain contains sequences complementary to specific regions in the pre-rRNA 35S. (**D**–**G**) Schematic representation of motifs $U3_{C'/D}$ and $U3_{B/C}$ present in U3 snoRNA from *Saccharomyces cerevisiae* and their respective consensus sequences in animals (34).

recruitment of the Nop56p/NOP56–Nop1p/FBL module (14–17).

The U3 snoRNP is an atypical box C/D snoRNP. Although it contains the 2′-*O*-methylase Nop1p/FBL, U3 snoRNP has never been shown to be a catalyst for rRNA 2′-*O*-methylation. U3 snoRNA pairs co-transcriptionally with the 35S/45S pre-rRNA, thus acting as an organizing chaperone to potentiate early cleavages at sites A0, A1 and A2 (18–26). This specialized function relies on the U3 snoRNA 5′ domain which base-pairs with several sequences of the 5′ external transcribed spacer (5′ ETS) and the 18S region (18,21,24,25,27–32). The U3 3′ domain contains four highly phylogenetically conserved sequences that form two non-conventional box C/D-like motifs, namely the C′/D and B/C motifs, named thereafter $U3_{C'/D}$ and $U3_{B/C}$, respectively (Figure 1C, D, E, F, and G) (9,33–36). In spite of some sequence divergences as compared with box C/D consensus sequence both $U3_{C'/D}$ and $U3_{B/C}$ bind Snu13p/SNU13 (9,34). However, Snu13p/SNU13 has a much higher affinity for $U3_{B/C}$ as compared to $U3_{C'/D}$ (9,34). Taking into account the fact that Snu13p/SNU13 is at the heart of box C/D snoRNP assembly, this raises the question of how the core U3 snoRNP is assembled.

Furthermore, another distinctive characteristic of the U3 snoRNP is the dissymmetry of protein assembly on the $U3_{C'/D}$ and $U3_{B/C}$ motifs. This is due to the presence of a specific U3 core protein Rrp9p in yeast and U3-55K in human (9,37–40), which is recruited on the $U3_{B/C}$ motif in a Snu13p/SNU13-dependent manner (41–44) together with Nop56p/NOP56 and Nop1p/FBL (45–49). In contrast, the classical set of C/D box proteins Snu13p, Nop58p and Nop1p is recruited on the $U3_{C'/D}$ motif (15,46,47). Nevertheless, as for conventional box C/D snoRNPs, it has been proposed that the two particles are connected through the Nop56p–Nop58p coiled-coil dimer. The cryo-EM structural determination of fungal early 90S pre-ribosomal particles, assembled at the 5′ end of the nascent pre-rRNA, have very recently confirmed this U3 snoRNP organization (45,48,49).

Assembly of box C/D snoRNPs is not an autonomous process *in vivo*, but requires *trans*-acting assembly factors (50–56) that include the protein Bcd1p/BCD1(ZNHIT6) (50,53,57,58), the heterodimer platform Rsa1p/NUFIP1–Hit1p/TRIP3 (50–54,59) and the HSP90-interacting complex R2TP that is composed of four proteins: the AAA^+ hexameric helicases Rvb1p/TIP49 (RUVBL1) and Rvb2p/TIP48 (RUVBL2), Tah1p/hSPAGH (RPAP3) and Pih1p/hPIH1 (PIH1D1, NOP17) (52,53,55,56,59–61). Rsa1p/NUFIP1 interacts with several proteins involved in box C/D snoRNP assembly (52,53). We recently identified amino acids required for the Snu13p–Rsa1p interaction

and showed that the snoRNA and Rsa1p interact with distinct faces of Snu13p (50,51).

In yeast, individual depletion of assembly factors Rsa1p, Hit1p, Pih1p and Rvb2p has little impact on U3 snoRNA steady state level (54,62). Nonetheless, their absence substantially impacts pre-rRNA processing, especially by slowing down cleavages at A0, A1 and A2 sites that is a hallmark of a U3 snoRNP functional defect (54). In addition, all of the assembly factors associate with U3 snoRNA precursors and are required for 3′-end processing of a truncated version of the U3 snoRNA (54). The U3 snoRNA from *Saccharomyces cerevisiae* is expressed from two independent genes *SNR17A* and *SNR17B* and follows a unique maturation pathway including intron splicing by the spliceosome (63), 3′-end trimming and cap hypermethylation (64). It was initially proposed that splicing as well as recruitment of core proteins occur after shorter 3′ extremities have been generated, i.e. at the +18 and +12 sites relative to 3′ end of the mature form (64). However, using reverse transcriptase-polymerase chain reaction (RT-PCR) analysis and less stringent conditions for protein immunoselection, we detected core proteins Nop1p, Nop56p and Nop58p, as well as main assembly factors Rsa1p, Hit1p and the R2TP complex in association with unspliced and spliced 3′-long precursors (54).

It was therefore of interest to determine how the C/D box specific assembly machinery adapts its mode of action in order to facilitate the peculiar U3 snoRNP biogenesis. As our previous data revealed the presence of Rsa1p on the early pre-U3 snoRNA precursors (54), we developed *in vivo* and *in vitro* analysis to decipher the role of this platform protein in pre-U3 snoRNP assembly. In agreement with the observation that altogether Rsa1p and Rrp9p contribute to maintain a high and stable level of U3 snoRNA *in vivo*, we found that Rsa1p and Rrp9p are simultaneously recruited on the Snu13p–$U3_{B/C}$ pre-snoRNP. Additionally, we show that Rsa1p enhances the affinity of Snu13p for the C′/D motif. RNA footprinting experiments and RNA binding assays suggest that this could occur by a direct contact of Rsa1p with the 5′ domain of U3. In addition, based on our published X-ray structure of a complex between Snu13p and a fragment of Rsa1p (50) and the recent cryo-EM structures of the U3 snoRNP in the 90S complex (45,48,49), our data provide insight into a possible additional function of Rsa1p consisting to prevent mature snoRNP formation and premature base paring of U3 with the pre-rRNA. Finally, as our results reveal that pre-U3 snoRNA splicing is an early step occurring prior to 3′-end maturation, we therefore propose a refined model for *S. cerevisiae* U3 snoRNP biogenesis.

MATERIALS AND METHODS

Plasmids and strains

The M13mp19::T7-snR17A (65) and M13mp19::T7-yU3AΔ2,3,4 (34) vectors were used as the templates to amplify by PCR the DNA fragments for T7 *in vitro* transcription of transcripts U3B/C and U3Δ2,3,4, respectively. Templates for production of wild type and variant yU3C′/D were obtained by hybridization of partially complementary oligonucleotides (34). To test *in vivo* the effects of mutations in RNA U3Δ2,3,4, we used recombinant plasmid pASZ11::U3Δ2,3,4 which is a truncated version of plasmid pASZ11::yU3A encoding the wild-type U3A snoRNA (25). Wild-type and variant pASZ11::U3Δ2,3,4 plasmids were transfected into *S. cerevisiae* strains JH84 (22), BY4741 and its knock out derivative Δ*RSA1* (54). The production of recombinant proteins Snu13 and $Rsa1_{230\text{-}381}$ were carried out using the bacterial expression vectors previously described, pGEX-6P-1::*SNU13* (34) and pGEX-6P-1::N3C1 (52), respectively. The ectopic expression of the wild-type and variant Rsa1p in yeast cells was carried out using the previously described yeast expression vectors pG1::*RSA1* and pG1::*RSA1*-R249/A (51). Expression vector pHXGWA::*RRP9*, encoding protein Rrp9 fused with thioredoxine (TRX) and a tag of 6 histidines (His_6TRX), was obtained by gateway technology (66). The *Escherichia coli* BL21(DE3)-CodonPlus strain was used for protein production.

Production of recombinant proteins

GST-Snu13p and GST-$Rsa1p_{230\text{-}381}$ proteins were purified from cell extract under native conditions, using Glutathione Sepharose 4B as recommended by the manufacturer (GE Healthcare). They were cleaved overnight on the beads using the PreScission protease (GE Healthcare). The recombinant His_6TRX-Rrp9 was purified using a 5 mL HisTrapTM HP column (GE Healthcare) and eluted with 0.5 M imidazole at pH 8. After imidazole elution or cleavage, proteins were dialyzed against buffer D (20 mM HEPES-KOH, pH 7.9; 150 mM KCl; 1.5 mM $MgCl_2$; 0.2 mM ethylenediaminetetraacetic acid (EDTA); 10% glycerol) and stored at −80°C.

His-pull down assays of *in vitro* assembled RNPs

Radiolabeled RNA (5000 cpm, ∼50 fmol) was incubated with various sets of recombinant proteins during 30 min in buffer D at 30°C, each protein was used at a final concentration of 1 μM. The RNP complexes formed were incubated with Nickel Sepharose beads (GE Healthcare) for 15 min at room temperature in 200 μl of binding buffer (10 mM Tris–HCl, pH 8.0; 150 mM NaCl; 0.1% octylphenoxypolyethoxyethanol (IGEPAL). The beads were washed three times for 10 min with 1 ml of binding buffer. RNAs were extracted by phenol–chloroform treatments, ethanol precipitated and fractionated on denaturing polyacrylamide gel.

Electrophoresis mobility shift assays (EMSA)

Yeast U3 and U14 box C/D snoRNAs were synthesized by *in vitro* transcription with T7 RNA polymerase using as the template a PCR fragment carrying the *S. cerevisiae* snoRNA coding sequence (34). After transcription, the RNA was 5′-end labeled with T4 polynucleotide kinase in the presence of [γ-^{32}P] (adenosinetriphosphate) ATP and purified by gel electrophoresis. For electrophoretic mobility shift assays (EMSA), ^{32}P-radiolabeled RNA (500 cpm, ∼5 fmol) was mixed with proteins at the concentration indicated in figure legends, in buffer D (20 mM HEPES-KOH,

pH 7.9; 150 mM KCl; 1.5 mM $MgCl_2$; 0.2 mM EDTA; 10% glycerol) and incubated for 20 min at 4°C. The RNA–protein complexes formed were resolved by native gel electrophoresis.

RNase footprinting assay

Radiolabeled RNA (5000 cpm, ∼50 fmol) and 1.5 μM for each protein were used for protein–RNA complexes formation under the conditions described above for EMSA. Ribonuclease (RNase) digestions of free and complexed RNAs were performed in 10 μl of buffer D for 6 min at 20°C with 0.8 U of T1 RNase (Roche), 2.4 U of T2 RNase (Gibco) or 0.001 U of V1 RNase (Kemotex). The reactions were stopped by addition of 100 μl of cold solution of yeast tRNA (200 ng/μl) and 100 μl of phenol/chloroform/isoamylic alcohol (25:24:1). Digestion products were extracted and precipitated with ethanol. An alkaline hydrolysis of RNAs was performed for 5 min at 96°C using 10 fmol of radiolabeled RNA with 100 mM sodium bicarbonate. A RNase T1 ladder was done by incubation of 10 fmol radiolabeled RNA in 1 M sodium hydroxide citrate in the presence of 2 μg tRNAs for 5 min at 65°C and then treated with 1 U of RNase T1 for 10 min at 65°C. The cleavage products were fractionated by electrophoresis on a 10% polyacrylamide–8 M urea gel.

Yeast handling and northern blot analyzes

Standard *S. cerevisiae* growth and handling techniques were employed. The *S. cerevisiae* Y190-Δ*RSA1* (*YPL193W::kanMX2*) strain was previously described (51). The *RSA1* knock-out strain obtained was transformed with plasmid pG1::*RSA1* encoding wild type (WT) or variant Rsa1p and grown in yeast extract peptone dextrose (YPD) medium. Total RNAs were extracted from exponentially growing cells (A_{600} ∼ 0.8). Northern-blots were carried on 5 μg of total RNA fractionated on polyacrylamide denaturing gels. After transfer to Zeta-Probe membrane (Biorad), RNAs were detected using specific 5′ ^{32}P-radiolabeled oligonucleotides probes NB-U3 (5′-CCGTCAGACTGTTCA-3′) and NB-U1 (5′-GACCAAGGAGTTTGCATCAATGA-3′).

Test of variant U3 snoRNA functionality

The *S. cerevisiae* strain JH84 transformed with pASZ11 and recombinant plasmid pASZ11::U3Δ2,3,4 and its variant derivative Δbulge was grown to stationary phase in (YPG) liquid medium containing galactose. After centrifugation and washing, the cells were transferred into liquid YPD medium containing glucose and grown a few hours before streaking on YPD solid medium. Samples were also streaked for growth control on YPG. Colonies were examined after 48 h of incubation at 30°C. The cellular stability of the variant U3Δ2,3,4 RNAs was studied by northern blot analysis as described in the previous section. The U6 snRNA level was used for standardization. RNAs were detected using specific 5′ ^{32}P-radiolabeled oligonucleotides probes NB-U3 and NB-U6 (5′-CAGGGGAACTGCTG-3′).

RNA co-IP (RIP) and RT-PCR analyzes

Yeast cells untagged or expressing TAP-tagged Rsa1p were grown in YPD medium and stopped during the logarithmic phase of growth (OD_{600} ∼ 0.8–1). Cells were lysed by bead-beating in breaking buffer; lysates were added to IgG-Sepharose beads (Sigma-Aldrich) and incubated 2 h at 4°C. Beads were washed four times in washing buffer. RNAs were extracted with phenol–chloroform and analyzed by RT-PCR. cDNAs were generated using the following primers:
(7517) CAGTGCAGGGTCCGAGGTATTCTGAA AACCAAACCTTTGG to detect the long pre-U3, (7515) GTCGTATCCAGTGCAGGGTCCGAGGTATTCGC ACTGGATACGACACAAAGGAA to detect the pre-U3 +18, (7514) GTCGTATCCAGTGCAGGGTCCGAG GTATTCGCACTGGATACGACACAAAAAGTGG to detect the pre-U3 +12, and (7424) GTCGTATCCA GTGCAGGGTCCGAGGTATTCGCACTGGATA CGACACTTGTC to detect form with the mature 3′-end. PCR were performed using the following primers: (7159) CAGTGCAGGGTCCGAGGTATT as constant reverse primer, (5252) TCTGTGTCGACGTACTTCA to detect the exon 1-containing species, and (5254) AGTCTTAGGTACTAGAGTTT to detect the intron-containing species.

3D modeling

To build the models of the U3 snoRNP from *Chaetomium thermophilum* and from *S. cerevisiae* with $Rsa1p_{239–265}$, we used software PyMOL 1.3 (67) to superimpose the crystal structure of the *S. cerevisiae* Snu13p-$Rsa1p_{239–265}$ ((50); PDB ID: 4NUT) to the cryo-EM structure of the U3 snoRNP in the *C. thermophilum* ((48) PDB ID: 5JPQ) and *S. cerevisiae* (49), PDB ID: 5WYJ and 5WYK) 90S pre-ribosomes.

RESULTS

Rsa1p is present all along pre-U3 processing including intron splicing before 3′-extension trimming

As yeast U3 snoRNP biogenesis includes several RNA maturation steps, before studying the role of Rsa1p in U3 snoRNP biogenesis, we used PCR approaches to precisely delineate the relative order of these processing steps (Figure 2). In a first series of experiments, cDNAs were primed by the RT_{long} oligonucleotide, which anneals downstream from the + 58 site (Figure 2A) and were amplified by PCR using a reverse primer (3′PCR) carrying the 5′ sequence of RT_{long} and two distinct forward primers that hybridize within the exon 1 (5′PCRa) and the intron (5′PCRb), respectively. After gel fractionation (Figure 2B), each PCR product was cloned and sequenced. Using 5′PCRa (upper panel), two minor bands corresponding to unspliced forms of long pre-U3A and pre-U3B were detected in the upper part of the gel, but the most abundant form was a shorter spliced product corresponding to spliced pre-U3 carrying the entire 3′ extension. These data illustrated the rapid elimination of the intron during the maturation process and confirmed the accumulation of spliced U3 precursors with a long 3′ extrem-

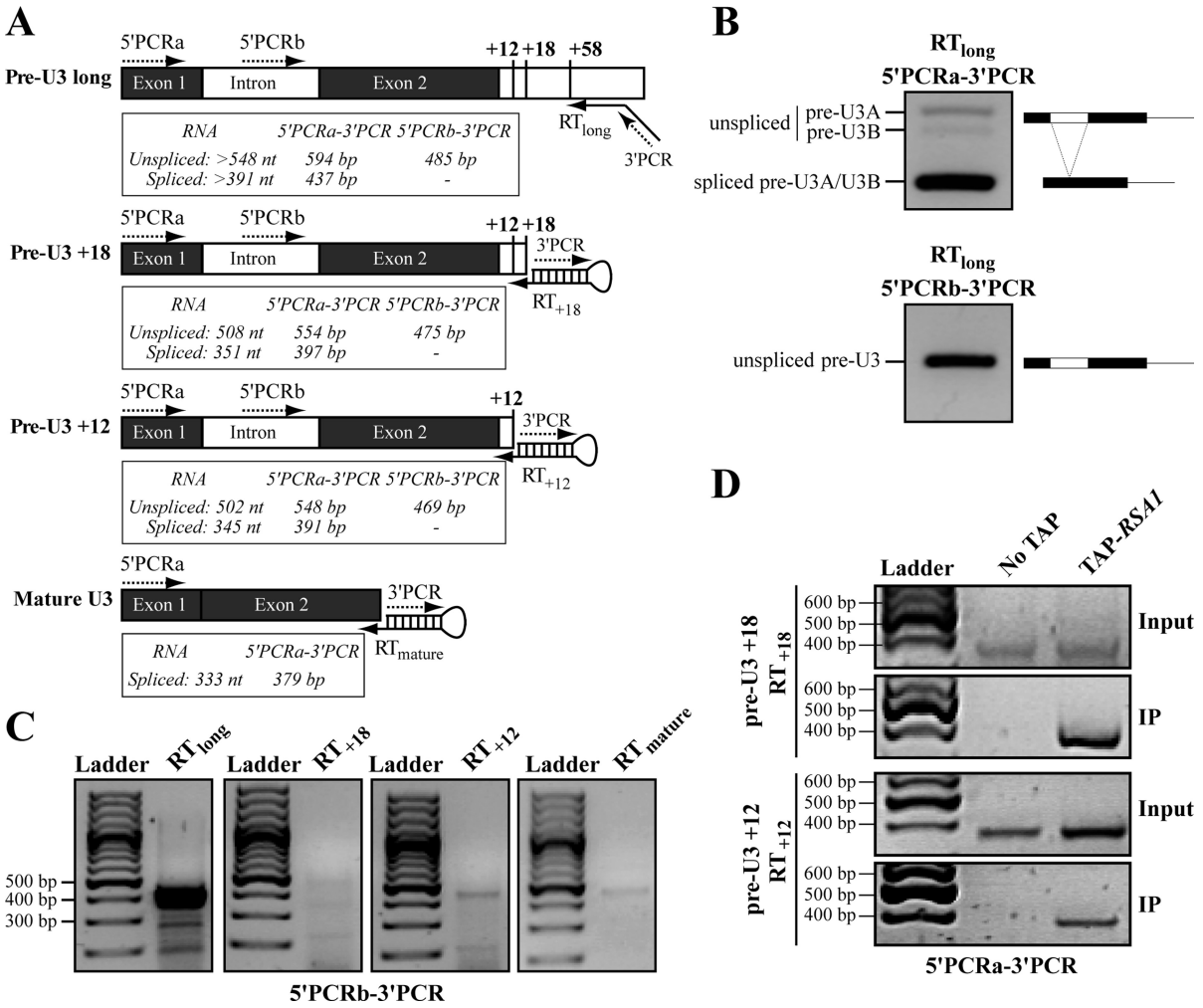

Figure 2. The U3 intron splicing occurs prior 3′-end nucleolytic maturation and Rsa1p remains associated with the latest pre-U3 intermediates. (**A**) Cartoon presenting the set of specific primers used for reverse transcriptase (RT) and polymerase chain reaction (PCR) steps in order to discriminate the maturation state at the 3′ extremity and the splicing status for each RNA species. The theoretical sizes of the RT-PCR products amplified with the various pairs of primers from the unspliced and spliced U3 RNAs are indicated (**B**) Detection by RT-PCR of the intronic sequence contained in the U3 snoRNA precursor which 3′ end is not processed. Reverse transcription was performed from a total RNA extract using the RT_{long} primer. PCR analyzes were performed using the primer couples 5′PCRa/3′PCR (upper panel) and 5′PCRb/3′PCR (lower panel), respectively. (**C**) Detection by RT-PCR of the intronic sequence in various 3′-end intermediates of the U3 snoRNA biogenesis pathway. RT was performed from a total RNA extract using the set of RT primers described in panel (A) and the primer couple 5′PCRb/3′PCR was used for PCR amplification. (**D**) Detection by RT-PCR of the U3 pre-snoRNA associated with Rsa1p. RNA co-immunoprecipitated with the fusion protein Rsa1-TAP endogenously expressed were primed for cDNA synthesis using the RT primers RT_{+18} and RT_{+12}, and then analyzed by PCR using the primer couple 5′PCRa/3′PCR. A strain without TAP-tagged protein expression was used as negative control.

ity. Therefore, the splicing reaction likely occurs before 3′-extension trimming. To obtain additional evidence for this possibility, we used a more sensitive and selective RT-PCR protocol (Supplementary Figure S1), which is based on reverse transcription primed by hairpin oligonucleotides designed to specifically and individually detect the 3′-end of the mature U3 and of the +12 and +18 pre-U3 RNAs (Supplementary Figure S1A and B). Indeed, a hairpin oligonucleotide primes the RT reaction at the 3′-end of RNA transcripts with a much higher affinity as compared to at an internal site (Supplementary Figure S1C). In addition, this hairpin primer-based RT-PCR protocol allowed detection of each U3 precursor molecules from a total RNA extract (Supplementary Figure S1D). Using this approach, we observed that only cDNAs primed with the primer specific to the entire 3′ extension led to the amplification of an abundant PCR product containing the intronic sequence (Figure 2C), confirming that intron removal occurs during the very early steps of U3 maturation, prior to 3′-end trimming. These data therefore provided new information on the chronology of events involved in yeast U3 snoRNA processing (64).

Then, using 3′-end selective hairpin primers for the RT and the primer hybridizing within exon 1 (5′PCRa) for the PCR, we detected that both spliced +18 and +12 pre-U3 RNAs were co-immunopurified with Rsa1p in yeast extracts (Figure 2D). This result demonstrated that association of Rsa1p, which occurs early on the nascent transcript (54), persists at least until the +12/+18 cleavage steps. Of note, both in the input and IP fractions no long PCR prod-

ucts corresponding to unspliced forms were detected, confirming the rapid elimination of the intron prior to 3′-end processing.

In vitro assembly of the $U3_{B/C}$ pre-RNP requires Snu13p and U3 helices 2, 3 and 4

Previous *in vivo* studies had shown the Snu13p/SNU13-dependent specific assembly of Rrp9p/U3-55K on the $U3_{B/C}$ motif both in *S. cerevisiae* and human cells (41,42). To test whether Rsa1p may play a role in this specific recruitment of Rrp9p we set up an *in vitro* assembly approach using the recombinant proteins Snu13 and His_6-tagged TRX-Rrp9 in combination with radiolabeled RNAs. Two truncated yeast U3 snoRNAs were used in these experiments, namely U3Δ2,3,4 and U3B/C (Figure 3A). The U3Δ2,3,4 RNA contains the $U3_{C'/D}$ and $U3_{B/C}$ motifs but lacks helices 2, 3 and 4 that surround the $U3_{B/C}$ motif. It was previously found to recruit Rrp9p on the $U3_{B/C}$ motif *in vivo* and to ensure cell growth after depletion of the endogenous U3 snoRNA (34,41). The U3B/C RNA contains helices 2, 3, 4 but lacks the 5′ domain and the C′/D motif. U14 snoRNA was used as a control to estimate the unspecific RNA binding property of Rrp9p. After complex formation, associated RNAs were co-purified with His_6TRX-Rrp9p on Nickel-Sepharose beads and analyzed by denaturing gel electrophoresis (Figure 3B). Incubation with Snu13p alone (lane 2) did not lead to RNA retention on the beads. Rrp9p interacted weakly and non-specifically with all three RNAs (lane 3). Snu13p addition increased significantly (∼3.6-fold) Rrp9p association with RNA U3B/C, but not with RNA U3Δ2,3,4 and the U14 snoRNA (lane 4). The positive effect of Snu13p on *in vitro* binding of Rrp9p to $U3_{B/C}$ in its authentic sequence context was confirmed by using the full length U3 snoRNA (Supplementary Figure S2). These data are in agreement with previous *in vitro* (44) and *in vivo* (41,42) findings. Furthermore, they underlined the importance of helices 2, 3 and 4 for *in vitro* binding of Rrp9p to the $U3_{B/C}$ motif, in spite that these helices are not essential for cell viability and Rrp9 binding *in vivo* (41,68). Interestingly also, UV-induced crosslinks of Rrp9p with helices 2 and 4 were previously detected by CRAC experiments suggesting an *in vivo* interaction of Rrp9p with these helices. Taken together the stronger requirements that we observed for *in vitro* assembly of Rrp9p compared to the *in vivo* situation may be explained by: (i) requirement for a $U3_{B/C}$ sequence environment more adapted to form a K-turn motif *in vitro* and (ii) a need for direct interaction of Rrp9p with surrounding helices to stabilize its interaction with this motif *in vitro*.

In vitro, $Rsa1p_{230–381}$ associates with the U3B/C–Snu13p–Rrp9p complex but is not required for its assembly

Next, to test for the possible effect of Rsa1p on Rrp9p *in vitro* assembly, the assembly assays were performed in the presence of the Rsa1p recombinant fragment spanning amino acids 230 to 381 ($Rsa1p_{230–381}$), which conserves the property of Rsa1p to interact with Snu13p and to promote box C/D snoRNP assembly (51,52). As evidenced by His-pull down assays, the addition of $Rsa1p_{230–381}$ had no major effect on the amount of RNA U3B/C retained on beads by His_6TRX-Rrp9 in the presence of Snu13p (Figure 3C, compare lane 3 with lane 4). This observation suggested that $Rsa1p_{230–381}$ does not promote nor prevent the incorporation of Rrp9p in the particle. To verify the presence of $Rsa1p_{230–381}$ in Rrp9p-containing particles, we next performed EMSA (Figure 3D). The complexes were formed in similar conditions as those analyzed in the His-pull down assay. As previously described (52), $Rsa1p_{230-381}$ cannot form a stable complex by direct interaction with a box C/D snoRNA *in vitro* (lane 4), but generated a supershift in the presence of Snu13p (RNP3 in lane 3). The addition of Rrp9p to RNA U3B/C led to a diffuse band shift (lane 5), suggesting a capacity of His_6TRX-Rrp9p to interact directly with the RNA. By contrast, a clearly defined band shift corresponding to a higher molecular weight complex was observed in the presence of Snu13p (RNP2 in lane 7) and a single complex (RNP4 in lane 8) was formed in the presence of $Rsa1p_{230–381}$, Snu13p and Rrp9p. Electrophoretic mobility of RNP4 was reduced compared to those of RNP3 (U3B/C–Snu13p–$Rsa1p_{230–381}$, lane 3) and RNP2 (U3B/C–Snu13p–Rrp9p, lane 7). This strongly suggested that association of Snu13p with RNA U3B/C and Rrp9p does not disturb the Snu13p–$Rsa1p_{230–381}$ interaction.

We previously showed that the Snu13p glutamate residue E_{72} is present at the Snu13p–Rsa1p interaction interface (50,51) and its substitution into an alanine abolishes formation of the Snu13p–Rsa1p complex (51). To reinforce the demonstration that Rrp9p recruitment does not rely on $Rsa1p_{230–381}$ *in vitro*, we repeated the U3B/C RNP *in vitro* assembly assays with the Snu13p variant E_{72}/A. Interestingly, the Snu13p variant E_{72}/A conserved its ability to enhance the recruitment of Rrp9p, both in the absence of the presence of $Rsa1p_{230–381}$ (Figure 3C). In agreement with this result, gel shift assays showed that this Snu13p variant conserves its property to bind RNA U3B/C (Figure 3E, lane 5 and (51)). The faster migration of the RNP1 complex formed with this variant protein is likely due to a protein conformational change as previously observed with the U14 snoRNA (51). A complex with a reduced electrophoretic mobility (RNP2 in Figure 3E, lane 6) was formed upon addition of both Rrp9p and Snu13p E_{72}/A indicating that the Snu13p variant did preserve its ability to enhance Rrp9p recruitment. Here again, the amount of associated Rrp9p was not modified upon $Rsa1p_{230–381}$ addition (Figure 3E, lane 7). Furthermore, the absence of $Rsa1p_{230–381}$ recruitment in the U3B/C-Snu13p–Rrp9p complexes formed with the E_{72}/A Snu13p variant indicated that Rrp9p by itself is not able to interact with $Rsa1p_{230–381}$. Altogether, we concluded that $Rsa1p_{230–381}$ is not required to assemble Rrp9p on the U3B/C particle *in vitro*. Moreover, the three proteins can be present together on the $U3_{B/C}$ motif as no antagonism between Rrp9p and Rsa1p was observed for their recruitment on the U3B/C–Snu13p pre-snoRNP.

In cell extract, residue R_{89} in Snu13p is required for Rrp9p recruitment

Rsa1p does not act alone in the box C/D assembly process, but in concert with several other cellular factors (50–

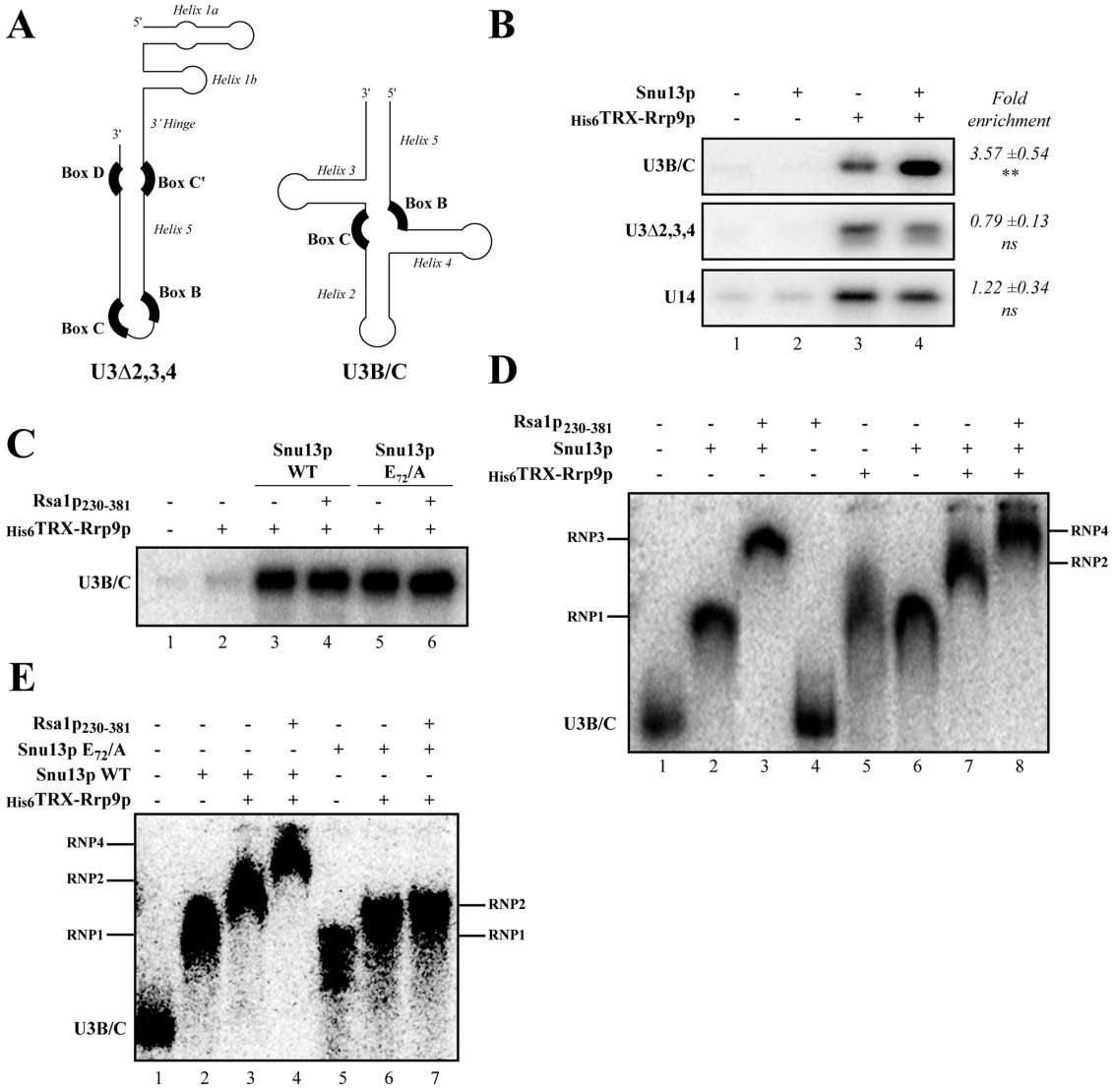

Figure 3. *In vitro* assembly of Rrp9p on $U3_{B/C}$ motif requires Snu13p and U3-helices 2, 3, 4 but not Rsa1p. (**A**) Schematic representation of the U3 snoRNA variants used for *in vitro* assembly. (**B**) *In vitro* assembly of Rrp9p-containing RNPs by His pull-down assays. Radiolabeled RNAs were incubated with the recombinant protein His_6TRX-Rrp9p in presence or absence of Snu13p. After incubation of this mixture with Ni-sepharose beads, RNAs retained on the beads were analyzed by denaturing gel electrophoresis. The U14 snoRNA was used as negative control for specificity. The fold enrichment represents the ratio of RNA co-purified with His_6TRX-Rrp9p in presence of Snu13p compared to the condition without Snu13p. Experiments have been done in triplicate. Student's *t*-test was used to calculate *P*-values (**$P \leq 0.01$, ns: non-significant). (**C**) The same experiment was carried out using the U3B/C RNA and with the additional presence of the recombinant $Rsa1p_{230–381}$ protein. The input corresponds to 10% of the total quantity of radiolabeled RNA used in the binding assays (left Lane). (D–E) *In vitro* assembly of various RNPs by electrophoretic mobility shift assays (EMSA). Radiolabeled U3B/C RNA was incubated with various combinations of recombinant Snu13p and its variant E_{72}/A, His_6TRX-Rrp9p and $Rsa1p_{230–381}$ each at a final concentration of 0.5 μM. The complexes formed were fractionated by gel electrophoresis. Positions of complexes Snu13p–U3B/C RNA (RNP1), Snu13p–His_6TRX-Rrp9p–U3-B/C RNA (RNP2), Snu13p–$Rsa1p_{230–381}$–U3-B/C RNA (RNP3) and Snu13p–His_6TRX-Rrp9p–$Rsa1p_{230–381}$–U3-B/C RNA (RNP4), as well as, of the free U3-B/C RNA (U14) are indicated on the sides of the autoradiogram.

54). To complete the demonstration, we designed a $U3_{B/C}$ RNP assembly assay based on yeast cellular extracts prepared from strain *GAL*::*SNU13* expressing (WT) or not Rsa1p (Δ*RSA1*) (Supplementary Figure S3). Cells were transformed with a plasmid expressing the ProtA-tagged Rrp9 protein. Before cell extract preparation, endogenous Snu13p expression was repressed by growth on glucose (Supplementary Figure S3A). For the assay, radiolabeled U3B/C RNA was pre-incubated or not with the recombinant Snu13p before incubation in the cellular extract. The RNAs associated with ProtA-Rrp9p were co-purified on IgG-Sepharose beads and analyzed by denaturing gel electrophoresis. As expected, a positive effect of Snu13p on the recruitment of Rrp9p on RNA U3B/C was observed in the presence or the absence of Rsa1p expression (Supplementary Figure S3A). As in the assays performed with purified proteins, the Snu13p variant E_{72}/A, which is unable to bind Rsa1p, conserved its property to enhance Rrp9p recruitment (Supplementary Figure S3B, lane 3). Interestingly, substitution by alanine of the Snu13p residue arginine

89 abolished the association of Rrp9p to RNA U3B/C in the extract (Supplementary Figure S3B, lane 4). Of note, previous data obtained using HeLa cell extract showed that a human SNU13 A_{88}/D and R_{91}/E double mutant, where R_{91} is the human counterpart of residue R_{89} mutated in our experiment has a very low capability to reinforce the recruitment of hU33-55K (the human counterpart of Rrp9p) on a human box B/C RNA (69). Furthermore, the R_{89} residue of Snu13p is essential for yeast cell growth since expression of the Snu13p R_{89}/A variant protein in *GAL*::*SNU13* WT was not able to rescue growth on glucose (data not shown).

Altogether, the data confirmed that Rsa1p has no stimulatory effect on the Snu13p-mediated binding of Rrp9p to the Snu13p–U3B/C complex and that Rrp9p association is strongly dependent on the presence of Snu13p residue R_{89}.

A positive effect of Rsa1p on RNP assembly on a U3 snoRNA variant binding Rrp9p with low efficiency *in vitro*

As discussed above, no significant impact on the U3 level was observed in a yeast deletion mutant of the *RSA1* gene (Δ*RSA1*) (52). However, we previously observed that the steady-state level of the mature form of the U3Δ2,3,4 RNA is lowered in a Δ*RSA1* strain and its 3′ extended precursors +12 and +18 accumulate (52). Based on these results and the above data showing that Rrp9p is not recruited *in vitro* on the U3Δ2,3,4 RNA (Figure 3B), we hypothesized that the effect of the *RSA1* disruption on U3Δ2,3,4 RNA maturation may result from the cumulative effect of Rsa1p depletion and the sub-optimal association of Rrp9p with this variant RNA. To test this hypothesis and since disruption of the *RSA1* gene could have pleiotropic effects, we used the R_{249}/A Rsa1p variant, which does not interact with Snu13p and cannot be recruited on the pre-snoRNP (51). The Δ*RSA1* yeast strain was complemented by ectopic expression of Rsa1p WT or the R_{249}/A variant (Figure 4). Total RNAs were extracted and analyzed by Northern-blot using U1 snRNA as internal control. The absence of endogenous Rsa1p led to an increase of the ratio between U3Δ2,3,4 precursors and the mature form (lane 2). Interestingly, ectopic expression of WT Rsa1p led to high production of mature U3Δ2,3,4 RNA (lane 3), while this was not the case for the R_{249}/A mutant (lane 4). The higher level of mature U3Δ2,3,4 RNA in the presence of Rsa1p might be explained by a higher kinetics of RNP assembly on the B/C and C′/D motifs. This effect is reinforced when Rsa1p is overexpressed, likely due to the limited number of Rsa1p molecules endogenously expressed in WT yeast cells as compared to the number of molecules of snoRNP core proteins (70). The present results confirmed that the recruitment of Rsa1p is a crucial event for production of fully matured U3Δ2,3,4 RNA. This need for Rsa1p may be explained by the presence of two suboptimal motifs in RNA U3Δ2,3,4: the $U3_{B/C}$ motif with truncated helices and the WT $U3_{C'/D}$ motif already shown to have a low affinity for Snu13p (K_d > 1500 nM for the small yU3C′/D RNA substrate) (34).

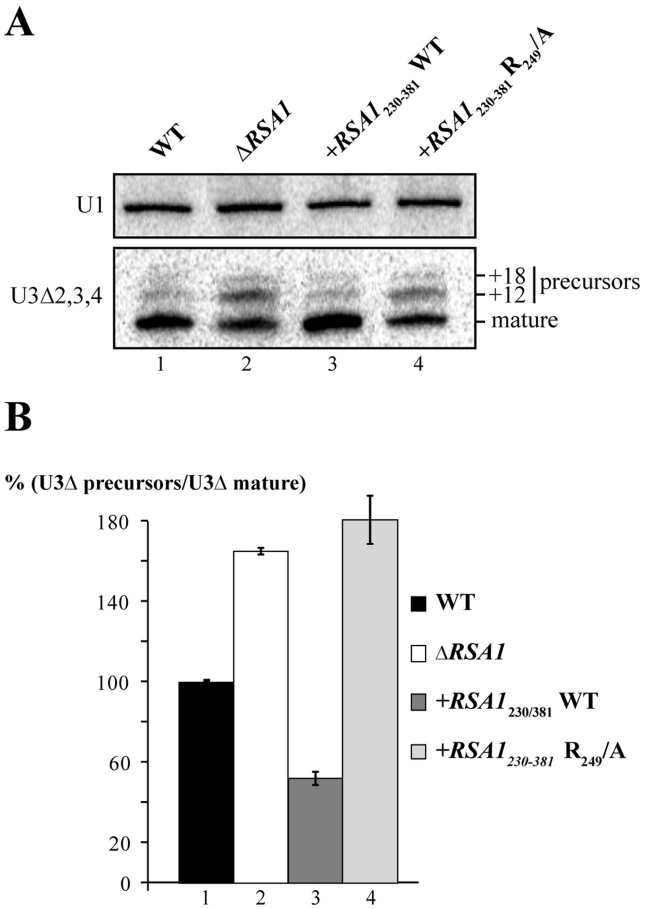

Figure 4. The absence of U3 helices 2, 3, 4 and Rsa1p affects the snoRNA level and pre-U3 processing. (**A**) Northern blot analysis of processing of the U3Δ2,3,4 variant RNA in WT and Δ*RSA1* mutant cells complemented by the wild-type Rsa1p or variant Rsa1p R_{249}/A, which is defective for interaction with Snu13p and to associate with a Snu13p-containing RNP (51). *RSA1* disruption and complementation by Rsa1p R_{249}/A are associated with a decrease in the cellular level of U3Δ2,3,4 and with the accumulation of its precursors cleaved at positions +12 or +18. U1 snRNA was used as a loading control. (**B**) Radioactivity in the bands of gel was quantified with the ImageQuant software after exposure of a phosphorimager screen. The signal of U3Δ2,3,4 precursors was divided by the signal of the mature U3Δ2,3,4. This ratio in WT strain is arbitrary considered as having a value of 100% and the ratios in other strains are expressed relative to this value. Error bars represent the standard deviation obtained from the mean value of three independent experiments.

Structural features explaining the low affinity of Snu13p for the yeast $U3_{C'/D}$ motif

Then, we tried to explain at the structural level why the yeast $U3_{C'/D}$ motif, which plays a key role in recruitment of the classical set of box C/D proteins and therefore for U3 nucleolar localization, has a low affinity for Snu13p. At the RNA level, the presence of a uridine nucleotide at position 2 (U_2) in the internal loop of the K-turn instead of a purine at this position in canonical box C/D motifs (Figure 1D and E) was already shown to decrease the affinity for Snu13p (34,47). Based on 3D structures established for archaeal L7Ae-box C/D RNA complexes (71) and the yeast Snu13p 3D structure (72), we postulated the formation of a stacking interaction between the guanidinium of the conserved argi-

nine 95 (R_{95}) in Snu13/SNU13 proteins and the purine at position 2 in canonical C/D motifs (Figure 5). Because of a U residue at position 2 in the yeast $U3_{C'/D}$ motif, the same interaction cannot be formed (Figure 5, compare panel A with panel B). However, residue R_{95} can establish a stabilizing interaction with the nucleobase of residue G1 which is almost universally conserved in U3 C′/D motifs (34). According to the recent cryo-EM structures established for the *S. cerevisiae* 90S processome (45,49), the Snu13p R_{95} amino acid points toward the nucleotides at positions 1 and 2 in the $U3_{C'/D}$ motif (Supplementary Figure S4), showing their close proximity.

To confirm the role of the Snu13p R_{95} residue in the Snu13p–$U3_{C'/D}$ interaction, we produced and purified the recombinant R_{95}/A Snu13p variant and used EMSA to compare the *in vitro* affinities of Snu13p WT and the Snu13p R_{95}/A variant for RNAs yU3C′/D WT, yU3C′/D U_2/A and yU3C′/D U_2/A+G_1/U. As expected the U_2/A substitution strongly reinforced binding of Snu13p WT (Figure 5C), while no binding of the Snu13p R_{95}/A variant to yU3C′/D WT was detected. The affinity of Snu13p WT for yU3C′/D U_2/A+G_1/U was almost identical to that for yU3C′/D WT showing the importance of the conserved G_1 residue. Taken together, the data confirm the general role of the conserved R_{95} residue in Snu13p binding to canonical C/D box snoRNA motifs. They explain why the $U3_{C'/D}$ motif with an uracil at position 2 has a low affinity for Snu13p and they point out the importance of an interaction between R_{95} in Snu13p and the conserved G_1 residue in the $U3_{C'/D}$ K-turn.

Rsa1p enhances the association of Snu13p with the suboptimal $U3_{C'/D}$ K-turn

Based on the suboptimal capability of the yeast $U3_{C'/D}$ motif to recruit Snu13p, it was of interest to look for the possible contribution of Rsa1p in $U3_{C'/D}$ RNP assembly. To assess the capacity of the recombinant $Rsa1p_{230–381}$ fragment to form a stable complex with Snu13p and the $U3_{C'/D}$ K-turn we first used the RNA U3Δ2,3,4 mutB variant. This RNA, which is defective for the $U3_{B/C}$ K-turn and possess only one Snu13p binding site, allowed us to visualize exclusively the complexes formed on $U3_{C'/D}$ (34) (Figure 6A). As expected, Snu13p had a very low affinity for the $U3_{C'/D}$ motif in this context (Figure 6B, top panel), detection of a retarded migration complex required a high concentration of Snu13p (at least ∼2 μM) and a total gel-shift required a Snu13p concentration of ∼4 μM. Interestingly, in the presence of $Rsa1p_{230–381}$, a retarded complex was observed at a lower Snu13p concentration (∼1.5 μM) (Figure 6B, middle panel). As negative control, no stimulation of Snu13p binding was observed upon addition of bovine serum albumin (BSA) (down panel). Therefore, the affinity of the Snu13p–$Rsa1p_{230–381}$ heterodimer for $U3_{C'/D}$ is higher than that of the monomeric Snu13p.

For more direct evidences of the positive effect of Rsa1p on $U3_{C'/D}$ pre-RNP formation, we performed RNA footprinting assays, using ribonucleases as probes. For this purpose, the 5′-end radiolabeled RNA U3Δ2,3,4 was incubated with T1, T2 or V1 ribonucleases and cleavage products were analyzed by electrophoresis on denaturing gel. Reproducible results were obtained in the course of several experiments and an example is illustrated in Figure 7. For each enzyme, treatments were performed on the naked RNA and after complex formation with Snu13p alone or in combination with $Rsa1p_{230–381}$. As the above experiment showed no binding of Snu13p to the $U3_{C'/D}$ motif at Snu13p concentrations below 2 μM (Figure 6B) and in order to detect only Snu13p binding driven by Rsa1p, we used a 1.5 μM concentration for both Snu13p and the $Rsa1p_{230–381}$ proteins. $U3_{B/C}$ for which Snu13p has a very high affinity (K_d < 75 nM) provided a positive control for Snu13p binding (34). In agreement with previous data obtained by chemical probing (34,41), the pre-incubation of Snu13p with the RNA led to a lower accessibility to RNases of phosphodiester bounds in box B (nucleotides from positions 108 to 117) and in box C (from positions 121 to 124 and between positions 125 and 126) (Figure 7B and C). Conversely, no protections were observed in the C′ box region in the presence of Snu13p alone, confirming that this protein is unable to stably interact with $U3_{C'/D}$ at a concentration of 1.5 μM (Figure 7A and C). Interestingly, the addition of $Rsa1p_{230–381}$ drastically changed the cleavage profiles, since several of the Snu13p specific protections (34) appeared in box C′ (phosphodiester bounds from positions 78 to 80 and 81 to 88). In agreement with the EMSA experiments, this result confirmed a higher binding of Snu13p on $U3_{C'/D}$ in the presence of Rsa1p.

Phosphodiester bonds outside of the C′/D and B/C motifs are also protected in the presence of Rsa1p

Interestingly, some of the phosphodiester bounds located downstream from the C′ box (between positions 91–92 and 94–96) were also cleaved to a lower extent in the presence of Rsa1p. Chemical probing of RNA U3Δ2,3,4 predicted that this region was single-stranded (34). However, the strong cleavage by RNase V1 between nucleotides C_{91} and A_{92} observed here suggests their possible involvement in a base-pair interaction or nucleobase stacking, as shown in Figure 7C. Two alternative conformations can indeed be proposed for this region of RNA U3Δ2,3,4. The protection of V1 cleavage 91–92 upon Snu13p–$Rsa1p_{230–381}$ binding on $U3_{C'/D}$ may reflect either an RNA conformational change toward the single-stranded conformation and/or a direct steric hindrance due to $Rsa1p_{230–381}$.

Some additional protections were also detected in box B in complexes formed in the presence of Rsa1p compared to Snu13p alone. Here again, they either result from steric hindrance linked to the presence of $Rsa1p_{230–381}$ or to stabilization of the $U3_{B/C}$–Snu13p complex by $Rsa1p_{230–381}$.

Finally, in the presence of Snu13p–$Rsa1p_{230–381}$, numerous other cleavages were reduced in regions outside the Snu13p binding sites. Additional protections against T2 and V1 RNases were detected in the 5′ domain of U3: in the segment from positions 36 to 60, in helix 1B and the 3′ hinge. These additional protections likely resulted from direct contacts of $Rsa1p_{230–381}$ with the RNA. In agreement with this hypothesis, we observed that the affinity of Snu13p for the RNA variant miniRNA U3Δ2,3,4-mutB lacking the 5′ domain was not enhanced in the presence of Rsa1p (Supplementary Figure S5). We concluded that additional contacts

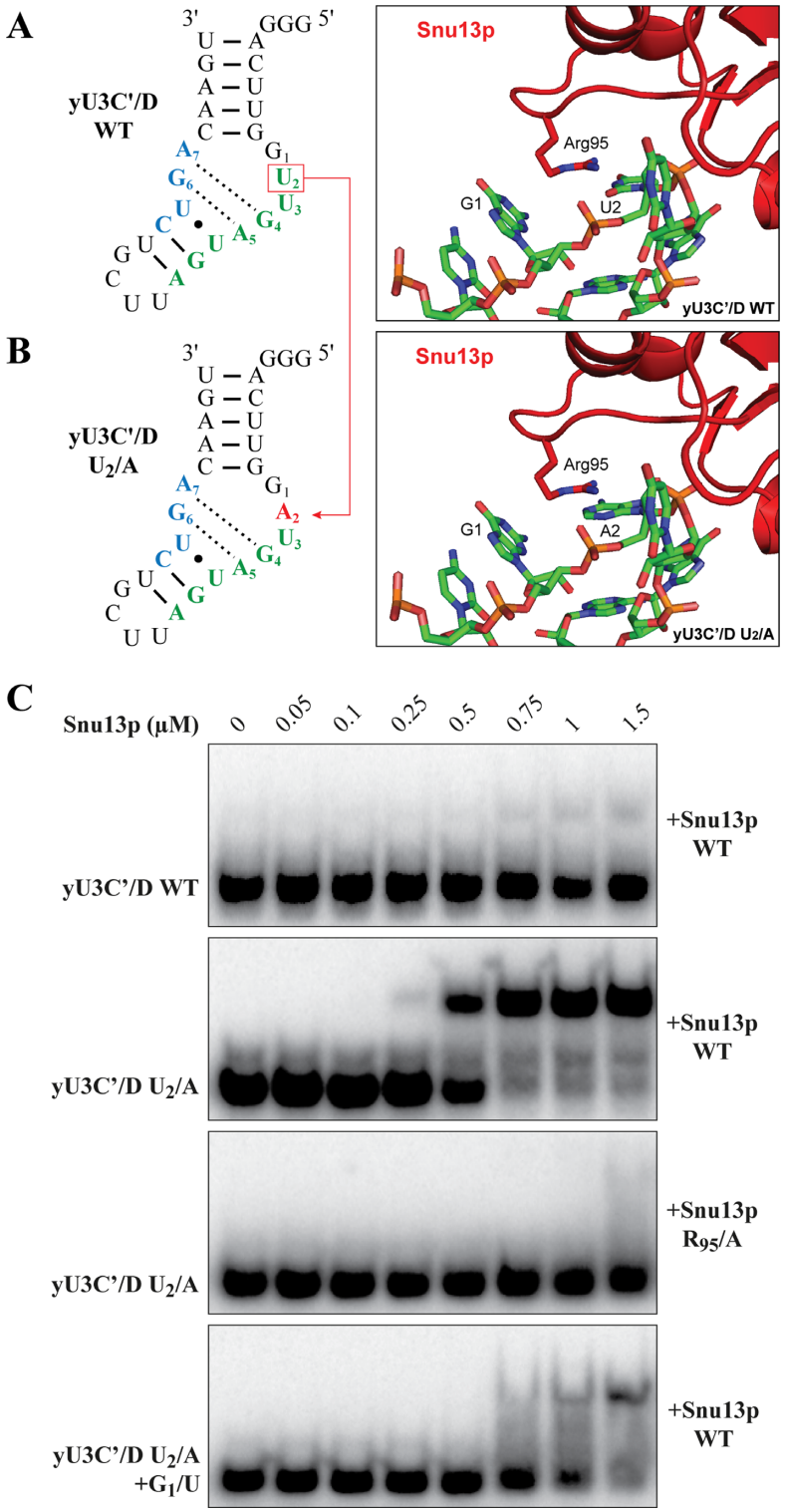

Figure 5. Uridine at position 2 in the $U3_{C'/D}$ K-turn weakens the stabilization by arginine R_{95} of the Snu13p–$U3_{C'/D}$ complex. (**A**) Schematic representation of the WT yU3C′/D RNA fragment used for EMSA (left) and magnified view (right) of a 3D model of the Snu13p–$U3_{C'/D}$ complex which was built on the basis of the known 3D structures of Snu13p ((72); PDB ID: 2ALE) and the archaeal complex L7Ae–box C/D sRNA ((71); PDB ID: 1RLG). (**B**) Same information for variant yU3C′/D U_2/A carrying the U_2/A substitution. (**C**) Formation of Snu13p–$U3_{C'/D}$ complex formation was analyzed by EMSA. Radiolabeled yU3C′/D WT and variant were incubated with increasing concentrations of recombinant wild-type or variant R_{95}/A Snu13p (indicated on the top of each lane).

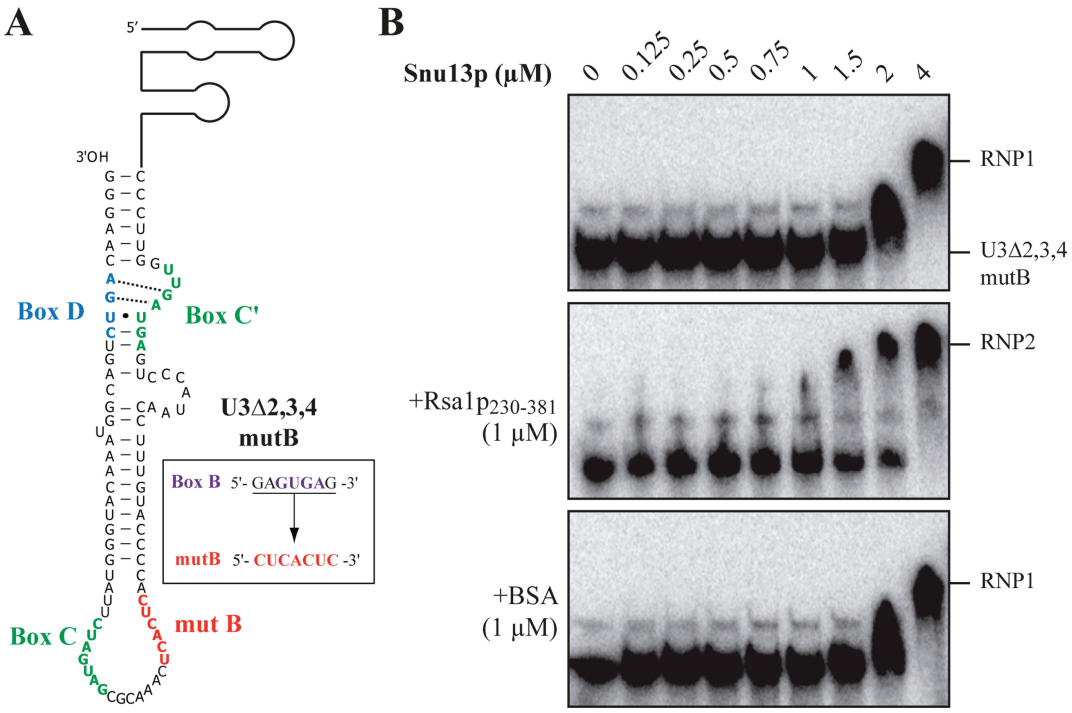

Figure 6. Rsa1p$_{230–381}$ increases the affinity for Snu13p–U3$_{C'/D}$ complex formation. (**A**) Schematic representation of the U3Δ2,3,4-mutB RNA used for EMSA. The box B was mutated to prevent the binding of Snu13p on U3$_{B/C}$. (**B**) *In vitro* assembly of Snu13p-containing RNPs analyzed by EMSA. Radiolabeled U3Δ2,3,4-mutB RNA was incubated with an increasing concentration of recombinant Snu13p (indicated on the top of each lane), in absence or in presence of Rsa1p$_{230–381}$ at a final concentration of 1 μM. Acetylated (bovine serum albumin) BSA at a final concentration of 1 μM was used for specificity control. The complexes formed were fractionated by non-denaturing gel electrophoresis.

of Rsa1p with the RNA molecule can occur in the 5′ region of U3 snoRNA and may contribute positively to U3$_{C'/D}$ pre-RNP assembly.

Rsa1p is predicted to mask key elements for U3 snoRNP assembly and function

Very recently, the structure of the 90S pre-ribosome of the hyperthermophilic yeast *C. thermophilum* and of *S. cerevisiae* were determined by cryo-EM allowing visualization of the U3 snoRNP 3D structure in its functional context (45,48,49). We superimposed the crystal structure of Snu13p–Rsa1p$_{239–265}$ heterodimer on the U3 snoRNP structures from *C. thermophilum* (Figure 8A) and *S. cerevisiae* (Supplementary Figure S6). Compared to Rsa1p$_{230–381}$ that was used in the footprinting experiments, the fragment of Rsa1p used for the X-ray crystallography lacks 116 amino acids at the C-terminal end and 9 residues at the N-terminal end (50). The overall model predicts that helix α2 of Rsa1p leads to two distinct steric clashes with Nop1p within the U3$_{C'/D}$ (Figure 8B and Supplementary Figure S6B) and U3$_{B/C}$ (Figure 8C and Supplementary Figure S6C) RNPs. In both cases the presence of Rsa1p is expected to prevent final placement of Nop1p in the mature RNP.

Moreover, the nucleotides at the base of box C′ and in the adjacent bulge loop, where protections were observed in the presence of Rsa1p$_{230–381}$, corresponds to a region located in close vicinity with Nop58p in the mature U3 snoRNP (Figure 8D and E; Supplementary Figure S6D). We attempted to test the contribution of this region in *in vivo* assembly of the U3Δ2,3,4 RNP by the design of a U3Δ2,3,4 RNA variant without the bulge (most of its nucleotides were deleted) that carried a stable continuous helix 5 (variant U3Δ2,3,4 Δbulge) (Figure 9). We paid attention to preserve the distance between the C′/D and B/C motifs in this variant RNA. Interestingly, while the WT U3Δ2,3,4 RNA is functional *in vivo*, ectopic expression of the Δbulge variant did not complement the absence of expression of the endogenous U3A snoRNA in JH84 *S. cerevisiae* cells (Figure 9B). Furthermore, northern blot analysis revealed a high instability of RNA U3Δ2,3,4 Δbulge *in vivo* (Figure 9C), what is a hallmark of incomplete box C/D snoRNP assembly, in particular of Nop58p association defect (13,73). Interestingly, the cryo-EM structure reveals that helix α9′ of Nop58p is inserted between the two RNA strands of the bulge, which likely locks Nop58p in the RNP (Figure 8D). Therefore, the presence of Rsa1p could control—by direct steric hindrance or by indirect long range effect on the RNA conformation—Nop58p placement in this U3 RNA region.

DISCUSSION

Proposition of a refined model for the U3 snoRNP biogenesis in *S. cerevisiae*

Taking into account the present results and new advances in the literature, we propose an updated model for the U3 snoRNP biogenesis pathway (Figure 10). Initially, Kufel *et al.*, proposed that the assembly of core proteins Nop1p, Nop56p and Nop58p, as well as the intron splicing, are late

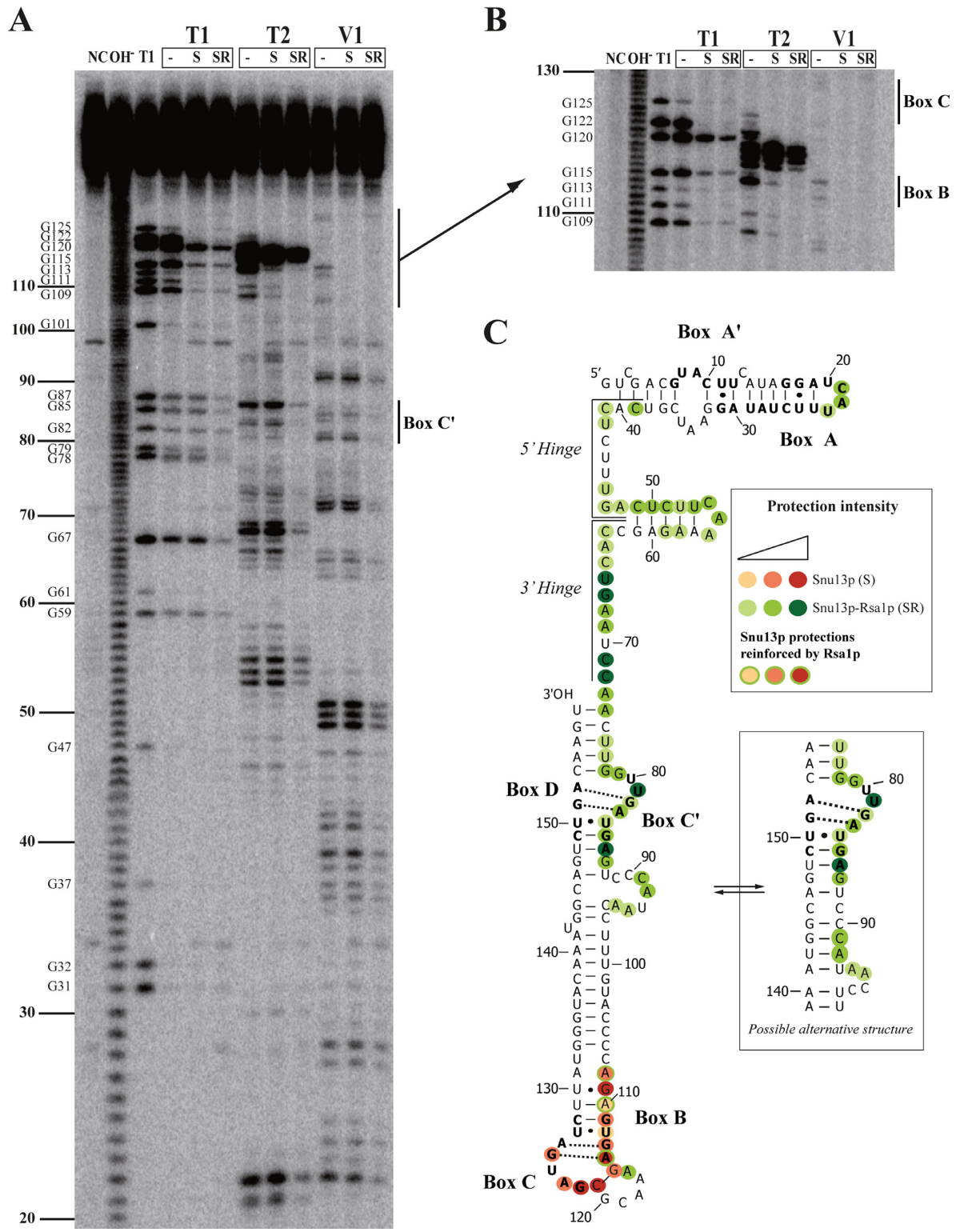

Figure 7. Rsa1p stabilizes the Snu13p binding on $U3_{C'/D}$ and contacts the 5′ domain of U3. (**A**) Digestion pattern of the U3Δ2,3,4 RNA by RNases T1, T2 and V1 on the naked RNA (−) or in presence of Snu13p (S) or Snu13p and $Rsa1p_{230–381}$ (SR). The size controls used are: none cut RNA (NC), alkaline hydrolysis ladder (OH^-) and denaturing T1 ladder (T1) revealing all the G nucleotides. T1 RNase cleaves preferentially at the 3′ extremity of unpaired G residues releasing 3′-phosphate and 5′-hydroxyl ends. T2 RNase hydrolyzes preferentially the simple strand region without a high specificity and releases 3′-phosphate and 5′-hydroxyl ends. V1 RNase cleaves preferentially double-strand regions or regions structured by base stacking releasing 3′-hydroxyl and 5′-phosphate ends. (**B**) More resolute view of $U3_{B/C}$ region obtained by a longer electrophoretic migration. (**C**) Positions on the U3Δ2,3,4 RNA of nucleotides protected against cleavages by the presence of Snu13p (in red) or Snu13p–$Rsa1p_{230–381}$ (in green). The intensity of the protection is relative to the color intensity (the darker tone representing the stronger protections). The insert shows a potential alternative secondary structure proximal to $U3_{C'/D}$.

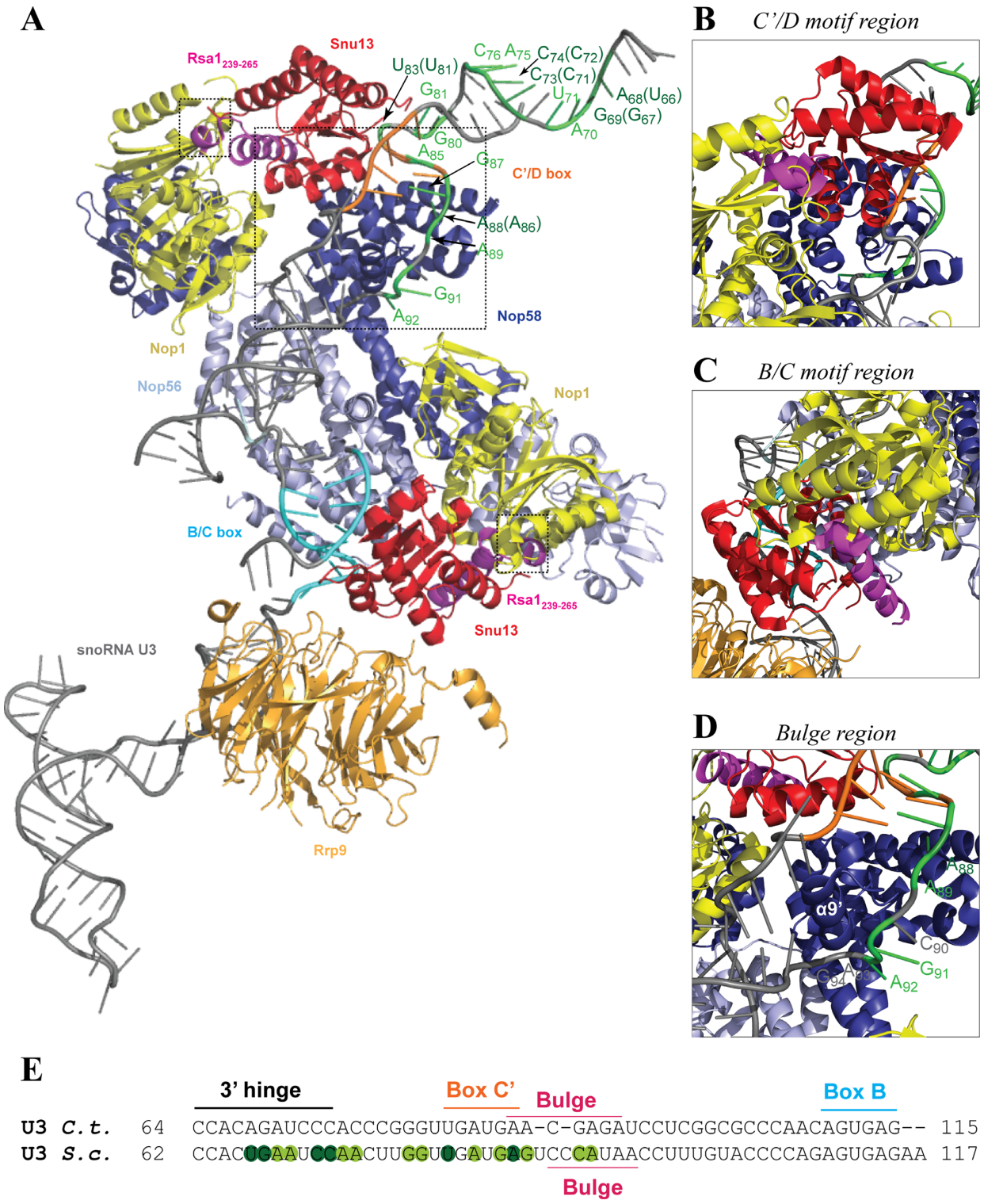

Figure 8. Rsa1p positioning in the U3 pre-small nucleolar ribonucleoprotein particles (snoRNP) is predicted to prevent the formation of the mature particle. (**A**) Ribbon representation of the U3 snoRNP within the 90S pre-ribosome from *Chaetomium thermophilum* ((48); PDB ID: 5JPQ) and superimposition with the crystal structure of complex Snu13p–Rsa1p$_{239–265}$ from *Saccharomyces cerevisiae* ((50); PDB ID: 4NUT). Proteins Snu13, Nop58, Nop56, Nop1 and Rrp9 are colored in red, dark blue, light blue, yellow and orange, respectively. The peptide Rsa1p$_{239–265}$ is colored in magenta. The backbone of U3 RNA is colored in gray. U3 RNA phosphodiester bonds protected against RNase cleavages by the presence of Snu13p–Rsa1p$_{230–381}$ are colored in green. The intensity of the protection is relative to the color intensity as in Figure 7. (**B**) Magnified view of the C′/D motif. (**C**) Magnified view of the B/C motif showing a distinct spatial hindrance with Rsa1p compared to the one observed on the C′/D motif. (**D**) Magnified view of Nop58p insertion between two the strands of helix II of the C′/D motif. The weakly phosphodiester bonds cleaved in the presence of Rsa1p$_{230–381}$ are colored in green. (**E**) Sequence alignment of the 5′ regions from *C. thermophilum* and *S. cerevisiae* U3 snoRNAs. Protection against RNase cleavages by the presence Snu13p–Rsa1p$_{230–381}$ are indicated with the same color code as in Figure 7.

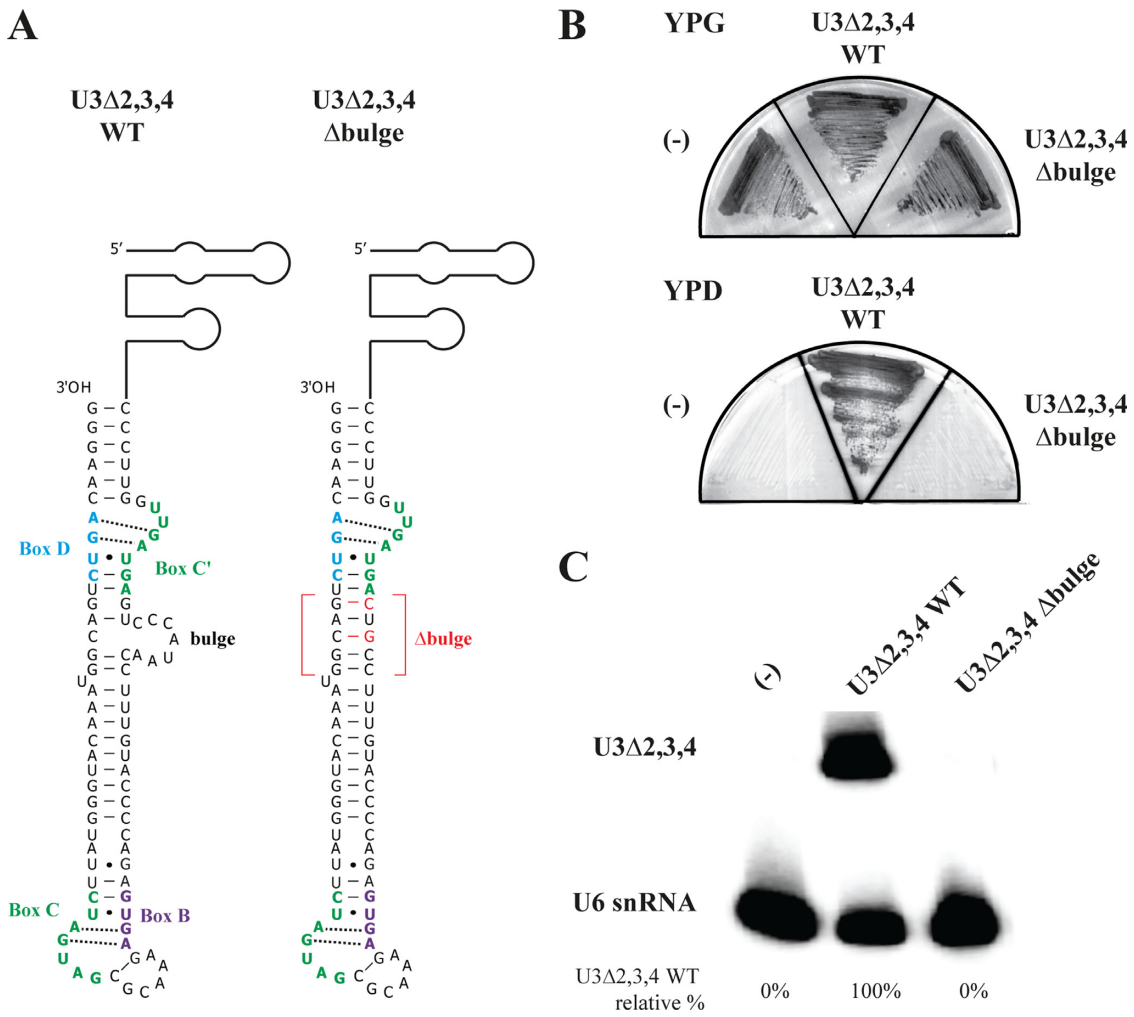

Figure 9. The box C′/D proximal bulge protected from RNases activity in the presence of Rsa1p$_{230–381}$ is essential for U3 snoRNP assembly and cell viability. (**A**) Schematic representation of the Δbulge variant of the U3Δ2,3,4 RNA. Introduced mutations are labeled in red. (**B**) Complementation assay in yeast strain JH84 (*GAL10*::*SNR17A*). In this strain, the galactose upstream activator sequence allows regulation of transcription of the U3 snoRNA encoding gene *SNR17A* whereas the second gene *SNR17B* encoding U3 is disrupted. The cells were transformed with pASZ11 plasmids: the empty vector (−) or the recombinant wild-type or variant Δbulge pASZ11::U3Δ2,3,4. Growth was tested on plates containing glucose (YPD) in order to block endogenous U3 expression. For control, the cells were also streaked on medium containing galactose (YPG). (**C**) Northern blot analysis of the amounts of U3 U3Δ2,3,4 RNAs. The U6 snRNA was used as a loading control. Radioactivity in the bands was quantified with the ImageQuant software after exposure of a phosphorimager screen. The signal of the U3Δ2,3,4 RNA was divided by the signal of the U6 snRNA and the ratio in cells expressing the WT U3Δ2,3,4 RNA was considered as having a value of 100%. Ratios of the two other strains are expressed relative to this value.

events occurring on the pre-U3 +18 and +12, which are products of a pre-U3 3′ end processing (64). In this model, the particle assembly was proposed to displace the Lsm proteins and Lhp1p from their binding site in order to favor the final 3′-end trimming by the exosome. In the present study, the RT-PCR reaction based on hairpin oligonucleotide-priming of cDNA synthesis revealed that the removal of the intron can occur on longest pre-U3s, prior the maturation of the 3′ extension (Figure 2). Furthermore, by using low stringency conditions, proteins Nop1p, Nop56p and Nop58p, as well as the assembly factors Rsa1p, Hit1p and the R2TP complex, were co-purified with unspliced and spliced forms of the long pre-U3 (54).

In the model presented here, the U3 snoRNP biogenesis starts with the early recruitment of the assembly machinery and core proteins (stage A). Lsm and Lhp1 proteins must also be recruited at this stage since they were detected in association with the unspliced pre-U3 (64,74). They are proposed to stabilize the 3′ extremity by preventing degradation by the exosome during particle assembly. After the binding of this set of proteins, the RNA maturation continues with the intron splicing (stage B), that could be coupled with the assembly process since the Cwc24 protein, which is required for the pre-U3 snoRNA splicing, interacts both with the splicing factor Cef1p and with the assembly factor Pih1p (75). After the splicing, the Rnt1p endonuclease allows the formation of the intermediates +58, +18 and +12, whose extremities are protected by Lhp1p and the Lsm proteins (stages C and D). The detection of Rsa1p at this stage suggests that +18/+12 RNPs are still in a pre-mature conformation that could correspond to the state of low stability described for the human U3 pre-snoRNPs

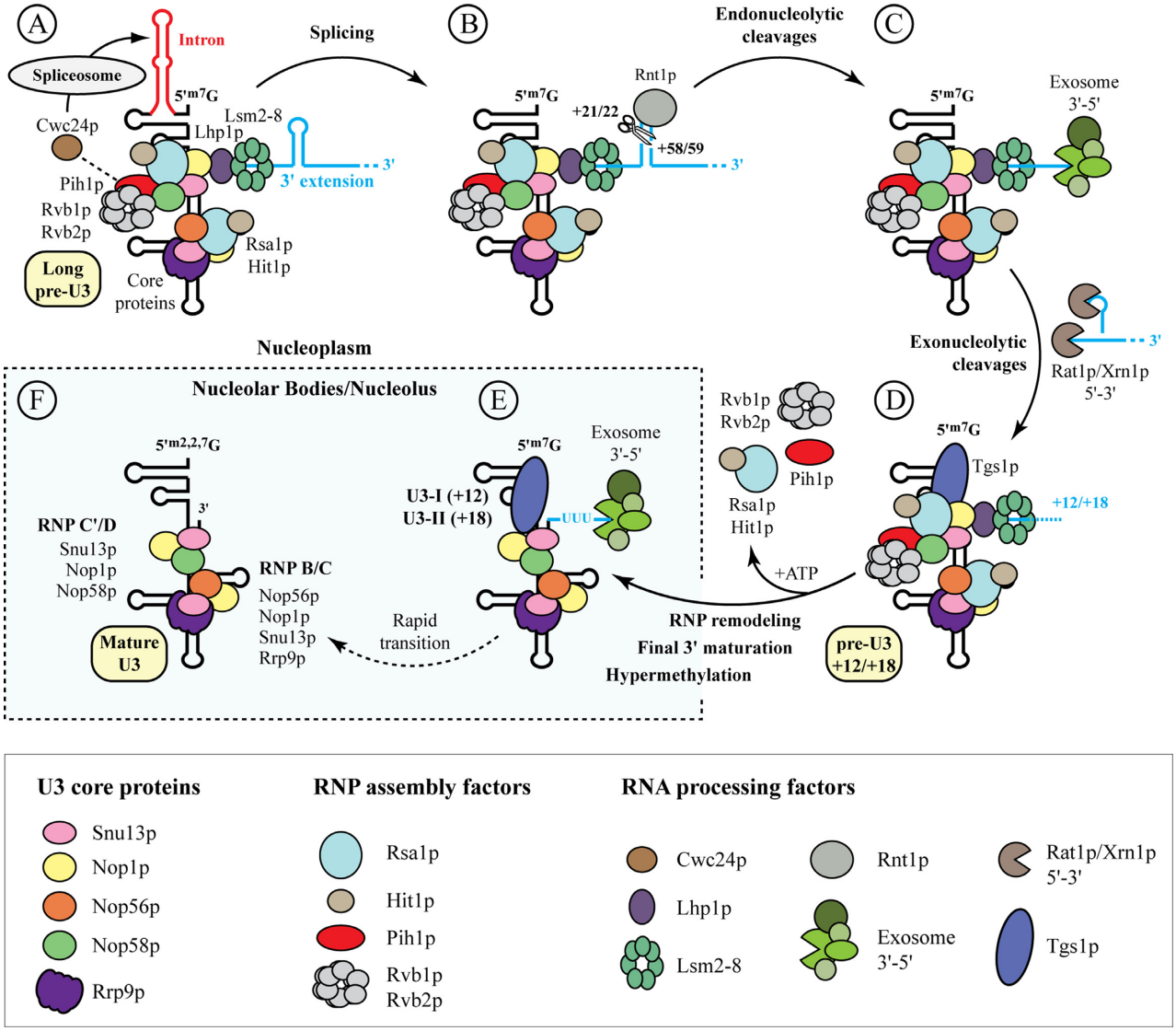

Figure 10. Refined model proposed for the biogenesis of the U3 snoRNP in *S. cerevisiae*. Explanations are given in the text.

(55). Indeed, the transition into the mature snoRNP may involve the ATPase activity of Rvb1p/Rvb2p during remodeling events leading to the release of the assembly machinery and the establishment of definitive interactions between snoRNP core proteins (stage E) (50,51,53,61). It is likely possible that the release of Lhp1p and the Lsm proteins occurs also at this stage giving rise to the final 3′-end trimming by the exosome. Furthermore, this late step may occur in the nucleolar bodies (NB), since the +18 and +12 intermediates were detected in these nucleolar corpuscles (76). Finally, the cap hypermethylation, (stage F) catalyzed by Tgs1p in the NB (76), may constitute the final step of the U3 snoRNA maturation, since only the 3′-end mature RNA is co-immunoprecipitated by hypermethylated-cap antibodies (64). Nevertheless, this step is possibly coupled with the assembly process, since the recruitment of the hypermethylase on the human U3 snoRNP was shown to occur at the pre-snoRNP level (55,77).

Rsa1p interacts with U3 5′ domain and stabilizes Snu13p on the sub-optimal $U3_{C'/D}$ K-turn

The data presented here highlight an unexpected feature of Rsa1p function in early U3 snoRNP assembly. Indeed, it is well established that $U3_{C'/D}$ constitutes a sub-optimal binding site for the Snu13/SNU13 protein, but nevertheless it efficiently assembles functional particles *in vivo* (9,34,47). Previous data have shown that the low affinity of Snu13p for $U3_{C'/D}$ results from the presence of an uracil at position 2 of the K-turn, while a purine is commonly found in other Snu13p/SNU13 binding K-turns (34) (Figure 1). Our present biochemical analysis explains this preference by the close proximity with the Arg95 residue of Snu13p. Indeed, the larger aromatic ring of a purine offers an optimal stacking surface that is much better stabilized by the guanidinium group of the arginine. Therefore, it is very likely that this intrinsic default must be compensated *in vivo* to allow the efficient assembly of the particle. Here, by using EMSA (Figure 6) and footprinting assays (Fig-

ure 7), we observed that Rsa1p assists Snu13p for $U3_{C'/D}$ binding. This activity may contribute to *in vivo* compensation for efficient $U3_{C'/D}$ RNP assembly. Moreover, additional protections from RNase cleavages were also observed nearby $U3_{C'/D}$ and in the U3 5′-functional domain upon addition of $Rsa1p_{230–381}$. Such modifications could result from changes in RNA conformation or from a lower accessibility for the RNases by Rsa1p hindering. Since these Rsa1p-associated protections are not correlated with appearance of new cleavages, it is unlikely that these changes arise from RNA folding modifications. In agreement with RNase protections induced by RNA–Rsa1p interaction, we found that the deletion of the 5′ domain totally disrupts the binding of Snu13p and Rsa1p on $U3_{C'/D}$ (Supplementary Figure S5). Hence, binding of Rsa1p with the U3 5′ domain may provide an anchor to stabilize binding of Snu13p on $U3_{C'/D}$.

In agreement with our previous studies (51,52) the present data show that the $Rsa1p_{230–381}$ fragment is not a stand-alone snoRNA binding protein (Figure 3D). In the absence of known RNA binding domain and given the relative weakness of Rsa1p RNA binding capacities, non-specific interactions are likely established between Rsa1p and the snoRNA U3 in the presence of Snu13p. Indeed, $Rsa1p_{230–381}$ is a highly basic protein with an isoelectric point of 10 well adapted for electrostatic contacts with the RNA phosphate backbone. Thereby, the combination of Snu13p and $Rsa1p_{230–381}$ may significantly increase the interaction surface between the protein complex and the snoRNA and thermodynamically favor the $U3_{C'/D}$ RNP formation.

Finally, the observation that Rsa1p interacts mainly with the 5′ domain is coherent with the fact that this part of the U3 snoRNA is not involved in interactions with specific partners at this step of the snoRNP biogenesis. U3 snoRNA maturation and its assembly into a snoRNP occur in the nucleoplasm, while its molecular function in pre-rRNA processing takes place in the nucleolus (76). To our knowledge, binding of the 5′ domain by additional core proteins happens exclusively in the nucleolus, once the snoRNP is incorporated in pre-ribosomal complexes. Indeed, several proteins, like Mpp10p, Imp3p and Imp4p, were shown to interact with heteroduplexes formed between U3 snoRNA 5′ domain and the pre-rRNA 35S/45S (21,24,78–80). Hence, as Rsa1p is not a nucleolar protein, the 5′ domain may be accessible for direct contacts with Rsa1p exclusively until U3 entry into the nucleolus. Furthermore, the large magnitude of the interaction interface between the 5′ domain and Rsa1p may mask putative binding sites to prevent interaction with unspecific binding proteins or nucleoplasmic RNAs.

Characterization of a $U3_{B/C}$ pre-snoRNP containing Rsa1p and both Rrp9 and Snu13 core proteins

Using recombinant proteins and a set of *in vitro* approaches, we showed that $Rsa1p_{230–381}$ has no influence on Rrp9p recruitment on the U3 snoRNA and that both proteins can simultaneously interact with the early Snu13p–RNA $U3_{B/C}$ complex (Figure 3C–D). These data are in agreement with previous mapping of the interaction sites at the surface of Snu13p/SNU13 (Supplementary Figure S7) and the recent 3D models of U3 snoRNP (48–51) showing that Rrp9p/55.5K and Rsa1p/NUFIP1 interact with independent regions on Snu13p. For example, arginine R_{91} of the human SNU13 protein (R_{89} for the *S. cerevisiae* Snu13p) was shown necessary for the recruitment of U3-55K onto the U3 snoRNP (69). In the 3D model of U3 snoRNP from *S. cerevisiae*, R_{89} points toward residues D_{323} and D_{403} present in a propeller loop of Rrp9p (Supplementary Figure S7). However, the Rsa1p/NUFIP1 binding site is distant and located on helix α3 of Snu13p/SNU13 containing residues E_{74}, D_{75} and K_{76} (E_{72}, D_{73} and K_{74} in *S. cerevisiae* Snu13p) (51). Furthermore, within the RNP, the RNA binding site for Rrp9p/U3-55K is located in close vicinity with helix I of the K-turn motif (45,48,49). In *S. cerevisiae*, it corresponds to the junction of the long U3-helices 2 and 4, whose physical contacts with Rrp9p were previously demonstrated by UV crosslinking (46) and whose deletion inhibits Rrp9p recruitment on a Snu13p–U3 RNA complex *in vitro* (Figure 3).

Effect of Rsa1p on mature U3 snoRNP assembly

The yeast U3 snoRNP 3D structural models deduced from the cryo-EM (45,48,49) have confirmed the predicted pseudo-symmetric model that was previously proposed for the U3 snoRNP organization (47). This model argues for the association of Snu13p/SNU13, Nop58p/NOP58 and Nop1p/FBL with $U3_{C'/D}$, while the second RNA motif $U3_{B/C}$ is bound by another set of proteins composed of Snu13p/SNU13, Rrp9p/U3-55K, Nop56p/NOP56 and Nop1p/FBL. Furthermore, as for the conventional box C/D snoRNPs, these two RNPs present on the U3 snoRNP are connected through the dimerization of the Nop56p/NOP56 and Nop58p/NOP58 coiled-coil domains. Given its ability to interact with the two copies of Snu13p positioned on both $U3_{C'/D}$ and $U3_{B/C}$, Rsa1p could influence the assembly of the C/D snoRNP proteins on both motifs.

Based on structural data on archaeal catalytic box C/D sRNP, it has previously been proposed that Snu13p–Rsa1p interaction would lead to a steric clash between the α2 helix of Rsa1p and the N-terminal domain of Nop58 that would prevent formation of the active conformation of the catalytic particle (50). Superimposition of Snu13p from the crystal structure of Snu13p–$Rsa1p_{239–265}$ on each Snu13p molecule in the *C. thermophilum* and *S. cerevisiae* cryo-EM structures reveals that Rsa1p would also interfere with formation of a mature and functional U3 snoRNP (Figure 8 and Supplementary Figure S6). Indeed, the α3 helix of Snu13p that contains the Rsa1p binding site overlaps with Nop1p binding site (48,49,51), such as the final positioning of Nop1p on both C′/D and B/C motifs could be hindered by Rsa1p (Figure 8B and C; Supplementary Figure S6B and C). Interestingly, in the *C. thermophilum* cryo-EM structure the two copies of Nop1p adopt a dissymmetric positioning (48). Hence, presence of Rsa1p on both $U3_{B/C}$ and $U3_{C'/D}$ would lead to distinct steric clashes: in $U3_{C'/D}$ Rsa1p helix α2 occupies the position of the loop between β6 and β7 strands and extremity of strand β7 of Nop1p, while in $U3_{B/C}$ it takes place of the loop β4–α4 and extremity of helix α4. Regarding the *S. cerevisiae* U3 snoRNP structure

(49), the two copies of Nop1p adopt a more similar position without being completely identical. In this context, Rsa1p helix α2 exhibits a steric clash with Nop1p helix α5 and the loop β4–α4 (in the same way as in the *C. thermophilum*) at the $U3_{C'/D}$ and $U3_{B/C}$ motifs, respectively. On the other hand, the presence of $Rsa1p_{230–381}$ also induced lower yields of RNase cleavages in the bulge formed by the extension of $U3_{C'/D}$ helix II (Figure 7C). This effect, which could result from a change of the local RNA conformation and/or a direct steric hindrance by $Rsa1p_{230–381}$, led us to pay a particular attention in this secondary structure element whose presence is highly conserved among U3 snoRNAs (34). Interestingly, the *C. thermophilum* U3 snoRNP structure highlights the importance of the bulge proximal to $U3_{C'/D}$ to lock the snoRNP assembly by close contacts with Nop58p whose helix α9′ is positioned across the central hole (48) (Figure 8D). This region is not defined in the *S. cerevisiae* cryo-EM structure (Supplementary Figure S6D). In the structure of archaeal catalytic box C/D sRNP the extremity of the NOP5 α9′ helix and its GAEK motif have been described as a key structural element to separate the antisense guide strand from the non-guide strand and to ensure accessibility to the targeted strand of the RNA substrate (81) (Supplementary Figure S8). Additionally, the two separated sRNA strands are stabilized by lengthwise interactions of their ribose–phosphate backbones with the dimeric coiled-coil domains of NOP5 (82) (Supplementary Figure S8D). By contrast, in *C. thermophilum* U3 snoRNP the Nop56p–Nop58p coiled-coil dimer is in a non-parallel orientation with the helix 5 separating the $U3_{B/C}$ and $U3_{C'/D}$ motifs (Supplementary Figure S8C). In such context, the surface of contact between the coiled-coil dimer and the snoRNA U3 is drastically reduced (by 2.4-fold). This substantial difference of stability between the two systems may be compensated by embedding the Nop58p α9′ helix into the $U3_{C'/D}$ proximal bulge. Indeed, we observed that the suppression of this bulge by a continuous helix 5 totally annihilates U3 stability and cell viability (Figure 9), what is a characteristic hallmark of a Nop58p assembly defect (13,73). Thus, this clamping of Nop58p into the bulge likely appears as a key step of the U3 snoRNP assembly and its obstruction by Rsa1p might also interfere with the final positioning of the core protein. Finally, $Rsa1p_{230–381}$ protects the U3–5′ domain and especially its 3′-hinge region (Figure 8A and E). Given the importance of the annealing of the 3′-hinge with the pre-rRNA 5′ ETS to nucleate the 90S pre-ribosome, it is conceivable that Rsa1p could directly promote or prevent formation of these base-pairing interactions. As Rsa1p is not a nucleolar protein, it is more likely that it acts as a shield to prevent premature interactions with this U3 domain. Interestingly, a recent study reporting the impact of various U3 mutations on yeast fitness has shown that the 5′ domain, the two K-turn motifs and their proximal sequences appear as the most affected (83). These effects are indisputably due to the role of these regions in the particle assembly and function; however it is interesting to note that Rsa1p protections are directed against these highly sensitive sequences. Rsa1p might preserve them from negative interferences. Altogether these data strongly suggest that Rsa1p might delay the formation of the functional particle. Similarly to Naf1p/NAF1 and Shq1p/SHQ1 in the box H/ACA snoRNP assembly pathway (84–86), Rsa1p might be a key factor to control the U3 snoRNP assembly timing and to maintain the particle in a pre-mature state until its final delivery into the 90S pre-ribosome.

To conclude, our present data indicate that Rsa1p role in snoRNP assembly may be more intricate than previously estimated. While its function as an assembly platform for box C/D snoRNP core protein is documented, its involvement in more subtle contacts with the snoRNA molecule was not shown before. Even if these interactions are weak and non-specific, they may substantially contribute to the proper assembly of Snu13p on sub-optimal K-turn motifs. Here, we demonstrate such an effect on the atypical box C′/D motif of the U3 snoRNA, but a future prospect is to extend this question to the C′/D′ motifs of other snoRNAs. Indeed, such investigations might help to understand the origin, the maintaining and the functioning of two dissimilar K-turn motifs (i.e. C/D and C′/D′) in the box C/D snoRNA family.

SUPPLEMENTARY DATA

Supplementary Data are available at NAR Online.

ACKNOWLEDGEMENTS

We thank the SCBIM platform of UL and FR BMCT CNRS 3209 for access to protein characterization facilities. Keqiong Ye is thanked for providing us information on the structure of the *S. cerevisiae* 90S pre-ribosome. Dr Simon Fortier is thanked for his advices during the manuscript preparation.

FUNDING

Centre National de la Recherche Scientifique (CNRS); University of Lorraine (UL); Agence Nationale de la Recherche [ANR-06-BLAN-0208; ANR-11-BSV8-01503]. French Ministère de l'Enseignement Supérieur et de la Recherche fellowship (to B.R., N.R.). Funding for open access: University of Lorraine and CNRS.
Conflict of interest statement. None declared.

REFERENCES

1. Henras,A.K., Plisson-Chastang,C., O'Donohue,M.F., Chakraborty,A. and Gleizes,P.E. (2015) An overview of pre-ribosomal RNA processing in eukaryotes. *Wiley Interdiscip. Rev. RNA*, **6**, 225–242.
2. Turowski,T.W. and Tollervey,D. (2015) Cotranscriptional events in eukaryotic ribosome synthesis. *Wiley Interdiscip. Rev. RNA*, **6**, 129–139.
3. Kressler,D., Hurt,E. and Bassler,J. (2010) Driving ribosome assembly. *Biochim. Biophys. Acta*, **1803**, 673–683.
4. Lafontaine,D.L. (2015) Noncoding RNAs in eukaryotic ribosome biogenesis and function. *Nat. Struct. Mol. Biol.*, **22**, 11–19.
5. Watkins,N.J. and Bohnsack,M.T. (2012) The box C/D and H/ACA snoRNPs: key players in the modification, processing and the dynamic folding of ribosomal RNA. *Wiley Interdiscip. Rev. RNA*, **3**, 397–414.
6. Decatur,W.A. and Fournier,M.J. (2003) RNA-guided nucleotide modification of ribosomal and other RNAs. *J. Biol. Chem.*, **278**, 695–698.
7. Kiss-Laszlo,Z., Henry,Y. and Kiss,T. (1998) Sequence and structural elements of methylation guide snoRNAs essential for site-specific ribose methylation of pre-rRNA. *EMBO J.*, **17**, 797–807.

8. Tycowski,K.T., Smith,C.M., Shu,M.D. and Steitz,J.A. (1996) A small nucleolar RNA requirement for site-specific ribose methylation of rRNA in Xenopus. *Proc. Natl. Acad. Sci. U.S.A.*, **93**, 14480–14485.
9. Watkins,N.J., Segault,V., Charpentier,B., Nottrott,S., Fabrizio,P., Bachi,A., Wilm,M., Rosbash,M., Branlant,C. and Luhrmann,R. (2000) A common core RNP structure shared between the small nucleoar box C/D RNPs and the spliceosomal U4 snRNP. *Cell*, **103**, 457–466.
10. Klein,D.J., Schmeing,T.M., Moore,P.B. and Steitz,T.A. (2001) The kink-turn: a new RNA secondary structure motif. *EMBO J.*, **20**, 4214–4221.
11. Vidovic,I., Nottrott,S., Hartmuth,K., Luhrmann,R. and Ficner,R. (2000) Crystal structure of the spliceosomal 15.5kD protein bound to a U4 snRNA fragment. *Mol. Cell*, **6**, 1331–1342.
12. Watkins,N.J., Dickmanns,A. and Luhrmann,R. (2002) Conserved stem II of the box C/D motif is essential for nucleolar localization and is required, along with the 15.5K protein, for the hierarchical assembly of the box C/D snoRNP. *Mol. Cell. Biol.*, **22**, 8342–8352.
13. Lafontaine,D.L. and Tollervey,D. (2000) Synthesis and assembly of the box C+D small nucleolar RNPs. *Mol. Cell. Biol.*, **20**, 2650–2659.
14. Aittaleb,M., Rashid,R., Chen,Q., Palmer,J.R., Daniels,C.J. and Li,H. (2003) Structure and function of archaeal box C/D sRNP core proteins. *Nat. Struct. Biol.*, **10**, 256–263.
15. Cahill,N.M., Friend,K., Speckmann,W., Li,Z.H., Terns,R.M., Terns,M.P. and Steitz,J.A. (2002) Site-specific cross-linking analyses reveal an asymmetric protein distribution for a box C/D snoRNP. *EMBO J.*, **21**, 3816–3828.
16. Szewczak,L.B., DeGregorio,S.J., Strobel,S.A. and Steitz,J.A. (2002) Exclusive interaction of the 15.5 kD protein with the terminal box C/D motif of a methylation guide snoRNP. *Chem. Biol.*, **9**, 1095–1107.
17. Szewczak,L.B., Gabrielsen,J.S., Degregorio,S.J., Strobel,S.A. and Steitz,J.A. (2005) Molecular basis for RNA kink-turn recognition by the h15.5K small RNP protein. *RNA*, **11**, 1407–1419.
18. Beltrame,M. and Tollervey,D. (1992) Identification and functional analysis of two U3 binding sites on yeast pre-ribosomal RNA. *EMBO J.*, **11**, 1531–1542.
19. Beltrame,M. and Tollervey,D. (1995) Base pairing between U3 and the pre-ribosomal RNA is required for 18S rRNA synthesis. *EMBO J.*, **14**, 4350–4356.
20. Borovjagin,A.V. and Gerbi,S.A. (1999) U3 small nucleolar RNA is essential for cleavage at sites 1, 2 and 3 in pre-rRNA and determines which rRNA processing pathway is taken in Xenopus oocytes. *J. Mol. Biol.*, **286**, 1347–1363.
21. Dutca,L.M., Gallagher,J.E. and Baserga,S.J. (2011) The initial U3 snoRNA:pre-rRNA base pairing interaction required for pre-18S rRNA folding revealed by in vivo chemical probing. *Nucleic Acids Res.*, **39**, 5180–5164.
22. Hughes,J.M. and Ares,M. Jr (1991) Depletion of U3 small nucleolar RNA inhibits cleavage in the 5′ external transcribed spacer of yeast pre-ribosomal RNA and impairs formation of 18S ribosomal RNA. *EMBO J.*, **10**, 4231–4239.
23. Kass,S., Tyc,K., Steitz,J.A. and Sollner-Webb,B. (1990) The U3 small nucleolar ribonucleoprotein functions in the first step of preribosomal RNA processing. *Cell*, **60**, 897–908.
24. Marmier-Gourrier,N., Clery,A., Schlotter,F., Senty-Segault,V. and Branlant,C. (2011) A second base pair interaction between U3 small nucleolar RNA and the 5′-ETS region is required for early cleavage of the yeast pre-ribosomal RNA. *Nucleic Acids Res.*, **39**, 9731–9745.
25. Mereau,A., Fournier,R., Gregoire,A., Mougin,A., Fabrizio,P., Luhrmann,R. and Branlant,C. (1997) An in vivo and in vitro structure-function analysis of the Saccharomyces cerevisiae U3A snoRNP: protein-RNA contacts and base-pair interaction with the pre-ribosomal RNA. *J. Mol. Biol.*, **273**, 552–571.
26. Osheim,Y.N., French,S.L., Keck,K.M., Champion,E.A., Spasov,K., Dragon,F., Baserga,S.J. and Beyer,A.L. (2004) Pre-18S ribosomal RNA is structurally compacted into the SSU processome prior to being cleaved from nascent transcripts in Saccharomyces cerevisiae. *Mol. Cell*, **16**, 943–954.
27. Beltrame,M., Henry,Y. and Tollervey,D. (1994) Mutational analysis of an essential binding site for the U3 snoRNA in the 5′ external transcribed spacer of yeast pre-rRNA. *Nucleic Acids Res.*, **22**, 4057–4065.
28. Borovjagin,A.V. and Gerbi,S.A. (2000) The spacing between functional Cis-elements of U3 snoRNA is critical for rRNA processing. *J. Mol. Biol.*, **300**, 57–74.
29. Borovjagin,A.V. and Gerbi,S.A. (2001) Xenopus U3 snoRNA GAC-Box A′ and Box A sequences play distinct functional roles in rRNA processing. *Mol. Cell. Biol.*, **21**, 6210–6221.
30. Brule,F., Venema,J., Segault,V., Tollervey,D. and Branlant,C. (1996) The yeast Hansenula wingei U3 snoRNA gene contains an intron and its coding sequence co-evolved with the 5′ ETS region of the pre-ribosomal RNA. *RNA*, **2**, 183–197.
31. Hartshorne,T. and Agabian,N. (1994) A common core structure for U3 small nucleolar RNAs. *Nucleic Acids Res.*, **22**, 3354–3364.
32. Hughes,J.M. (1996) Functional base-pairing interaction between highly conserved elements of U3 small nucleolar RNA and the small ribosomal subunit RNA. *J. Mol. Biol.*, **259**, 645–654.
33. Hughes,J.M., Konings,D.A. and Cesareni,G. (1987) The yeast homologue of U3 snRNA. *EMBO J.*, **6**, 2145–2155.
34. Marmier-Gourrier,N., Clery,A., Senty-Segault,V., Charpentier,B., Schlotter,F., Leclerc,F., Fournier,R. and Branlant,C. (2003) A structural, phylogenetic, and functional study of 15.5-kD/Snu13 protein binding on U3 small nucleolar RNA. *RNA*, **9**, 821–838.
35. Tycowski,K.T., Shu,M.D. and Steitz,J.A. (1993) A small nucleolar RNA is processed from an intron of the human gene encoding ribosomal protein S3. *Genes Dev.*, **7**, 1176–1190.
36. Wise,J.A. and Weiner,A.M. (1980) Dictyostelium small nuclear RNA D2 is homologous to rat nucleolar RNA U3 and is encoded by a dispersed multigene family. *Cell*, **22**, 109–118.
37. Granneman,S., Vogelzangs,J., Luhrmann,R., van Venrooij,W.J., Pruijn,G.J. and Watkins,N.J. (2004) Role of pre-rRNA base pairing and 80S complex formation in subnucleolar localization of the U3 snoRNP. *Mol. Cell. Biol.*, **24**, 8600–8610.
38. Lubben,B., Marshallsay,C., Rottmann,N. and Luhrmann,R. (1993) Isolation of U3 snoRNP from CHO cells: a novel 55 kDa protein binds to the central part of U3 snoRNA. *Nucleic Acids Res.*, **21**, 5377–5385.
39. Lukowiak,A.A., Granneman,S., Mattox,S.A., Speckmann,W.A., Jones,K., Pluk,H., Venrooij,W.J., Terns,R.M. and Terns,M.P. (2000) Interaction of the U3-55k protein with U3 snoRNA is mediated by the box B/C motif of U3 and the WD repeats of U3-55k. *Nucleic Acids Res.*, **28**, 3462–3471.
40. Venema,J., Vos,H.R., Faber,A.W., van Venrooij,W.J. and Raue,H.A. (2000) Yeast Rrp9p is an evolutionarily conserved U3 snoRNP protein essential for early pre-rRNA processing cleavages and requires box C for its association. *RNA*, **6**, 1660–1671.
41. Clery,A., Senty-Segault,V., Leclerc,F., Raue,H.A. and Branlant,C. (2007) Analysis of sequence and structural features that identify the B/C motif of U3 small nucleolar RNA as the recognition site for the Snu13p-Rrp9p protein pair. *Mol. Cell. Biol.*, **27**, 1191–1206.
42. Granneman,S., Pruijn,G.J., Horstman,W., van Venrooij,W.J., Luhrmann,R. and Watkins,N.J. (2002) The hU3-55K protein requires 15.5K binding to the box B/C motif as well as flanking RNA elements for its association with the U3 small nucleolar RNA in Vitro. *J. Biol. Chem.*, **277**, 48490–48500.
43. Pluk,H., Soffner,J., Luhrmann,R. and van Venrooij,W.J. (1998) cDNA cloning and characterization of the human U3 small nucleolar ribonucleoprotein complex-associated 55-kilodalton protein. *Mol. Cell. Biol.*, **18**, 488–498.
44. Zhang,L., Lin,J. and Ye,K. (2013) Structural and functional analysis of the U3 snoRNA binding protein Rrp9. *RNA*, **19**, 701–711.
45. Chaker-Margot,M., Barandun,J., Hunziker,M. and Klinge,S. (2017) Architecture of the yeast small subunit processome. *Science*, **355**, eaal1880.
46. Granneman,S., Kudla,G., Petfalski,E. and Tollervey,D. (2009) Identification of protein binding sites on U3 snoRNA and pre-rRNA by UV cross-linking and high-throughput analysis of cDNAs. *Proc. Natl. Acad. Sci. U.S.A.*, **106**, 9613–9618.
47. Knox,A.A., McKeegan,K.S., Debieux,C.M., Traynor,A., Richardson,H. and Watkins,N.J. (2011) A weak C′ box renders U3 snoRNA levels dependent on hU3-55K binding. *Mol. Cell. Biol.*, **31**, 2404–2412.
48. Kornprobst,M., Turk,M., Kellner,N., Cheng,J., Flemming,D., Kos-Braun,I., Kos,M., Thoms,M., Berninghausen,O., Beckmann,R. *et al.* (2016) Architecture of the 90S pre-ribosome: a structural view on the birth of the eukaryotic ribosome. *Cell*, **166**, 380–393.

49. Sun,Q., Zhu,X., Qi,J., An,W., Lan,P., Tan,D., Chen,R., Wang,B., Zheng,S., Zhang,C. *et al.* (2017) Molecular architecture of the 90S small subunit pre-ribosome. *Elife*, **6**, e22086.
50. Bizarro,J., Charron,C., Boulon,S., Westman,B., Pradet-Balade,B., Vandermoere,F., Chagot,M.E., Hallais,M., Ahmad,Y., Leonhardt,H. *et al.* (2014) Proteomic and 3D structure analyses highlight the C/D box snoRNP assembly mechanism and its control. *J. Cell. Biol.*, **207**, 463–480.
51. Rothe,B., Back,R., Quinternet,M., Bizarro,J., Robert,M.C., Blaud,M., Romier,C., Manival,X., Charpentier,B., Bertrand,E. *et al.* (2014) Characterization of the interaction between protein Snu13p/15.5K and the Rsa1p/NUFIP factor and demonstration of its functional importance for snoRNP assembly. *Nucleic Acids Res.*, **42**, 2015–2036.
52. Boulon,S., Marmier-Gourrier,N., Pradet-Balade,B., Wurth,L., Verheggen,C., Jady,B.E., Rothe,B., Pescia,C., Robert,M.C., Kiss,T. *et al.* (2008) The Hsp90 chaperone controls the biogenesis of L7Ae RNPs through conserved machinery. *J. Cell Biol.*, **180**, 579–595.
53. McKeegan,K.S., Debieux,C.M., Boulon,S., Bertrand,E. and Watkins,N.J. (2007) A dynamic scaffold of pre-snoRNP factors facilitates human box C/D snoRNP assembly. *Mol. Cell. Biol.*, **27**, 6782–6793.
54. Rothe,B., Saliou,J.M., Quinternet,M., Back,R., Tiotiu,D., Jacquemin,C., Loegler,C., Schlotter,F., Pena,V., Eckert,K. *et al.* (2014) Protein Hit1, a novel box C/D snoRNP assembly factor, controls cellular concentration of the scaffolding protein Rsa1 by direct interaction. *Nucleic Acids Res.*, **42**, 10731–10747.
55. Watkins,N.J., Lemm,I., Ingelfinger,D., Schneider,C., Hossbach,M., Urlaub,H. and Luhrmann,R. (2004) Assembly and maturation of the U3 snoRNP in the nucleoplasm in a large dynamic multiprotein complex. *Mol. Cell*, **16**, 789–798.
56. Zhao,R., Kakihara,Y., Gribun,A., Huen,J., Yang,G., Khanna,M., Costanzo,M., Brost,R.L., Boone,C., Hughes,T.R. *et al.* (2008) Molecular chaperone Hsp90 stabilizes Pih1/Nop17 to maintain R2TP complex activity that regulates snoRNA accumulation. *J. Cell Biol.*, **180**, 563–578.
57. Bragantini,B., Tiotiu,D., Rothe,B., Saliou,J.M., Marty,H., Cianferani,S., Charpentier,B., Quinternet,M. and Manival,X. (2016) Functional and structural insights of the Zinc-Finger HIT protein family members involved in Box C/D snoRNP biogenesis. *J. Mol. Biol.*, **428**, 2488–2506.
58. Peng,W.T., Robinson,M.D., Mnaimneh,S., Krogan,N.J., Cagney,G., Morris,Q., Davierwala,A.P., Grigull,J., Yang,X., Zhang,W. *et al.* (2003) A panoramic view of yeast noncoding RNA processing. *Cell*, **113**, 919–933.
59. Quinternet,M., Rothe,B., Barbier,M., Bobo,C., Saliou,J.M., Jacquemin,C., Back,R., Chagot,M.E., Cianferani,S., Meyer,P. *et al.* (2015) Structure/function analysis of protein-protein interactions developed by the yeast Pih1 platform protein and its partners in box C/D snoRNP assembly. *J. Mol. Biol.*, **427**, 2816–2839.
60. Back,R., Dominguez,C., Rothe,B., Bobo,C., Beaufils,C., Morera,S., Meyer,P., Charpentier,B., Branlant,C., Allain,F.H. *et al.* (2013) High-resolution structural analysis shows how Tah1 tethers Hsp90 to the R2TP complex. *Structure*, **21**, 1834–1847.
61. McKeegan,K.S., Debieux,C.M. and Watkins,N.J. (2009) Evidence that the AAA+ proteins TIP48 and TIP49 bridge interactions between 15.5K and the related NOP56 and NOP58 proteins during box C/D snoRNP biogenesis. *Mol. Cell. Biol.*, **29**, 4971–4981.
62. King,T.H., Decatur,W.A., Bertrand,E., Maxwell,E.S. and Fournier,M.J. (2001) A well-connected and conserved nucleoplasmic helicase is required for production of box C/D and H/ACA snoRNAs and localization of snoRNP proteins. *Mol. Cell. Biol.*, **21**, 7731–7746.
63. Myslinski,E., Segault,V. and Branlant,C. (1990) An intron in the genes for U3 small nucleolar Rnas of the yeast Saccharomyces-Cerevisiae. *Science*, **247**, 1213–1216.
64. Kufel,J., Allmang,C., Chanfreau,G., Petfalski,E., Lafontaine,D.L. and Tollervey,D. (2000) Precursors to the U3 small nucleolar RNA lack small nucleolar RNP proteins but are stabilized by La binding. *Mol. Cell. Biol.*, **20**, 5415–5424.
65. Segault,V., Mougin,A., Gregoire,A., Banroques,J. and Branlant,C. (1992) An experimental study of Saccharomyces cerevisiae U3 snRNA conformation in solution. *Nucleic Acids Res.*, **20**, 3443–3451.
66. Busso,D., Delagoutte-Busso,B. and Moras,D. (2005) Construction of a set gateway-based destination vectors for high-throughput cloning and expression screening in Escherichia coli. *Anal. Biochem.*, **343**, 313–321.
67. DeLano,W.L. (2010) *The PyMOL Molecular Graphics System, Version 1.3r1*. Schrödinger, LLC, NY.
68. Samarsky,D.A. and Fournier,M.J. (1998) Functional mapping of the U3 small nucleolar RNA from the yeast Saccharomyces cerevisiae. *Mol. Cell. Biol.*, **18**, 3431–3444.
69. Schultz,A., Nottrott,S., Watkins,N.J. and Luhrmann,R. (2006) Protein-protein and protein-RNA contacts both contribute to the 15.5K-mediated assembly of the U4/U6 snRNP and the box C/D snoRNPs. *Mol. Cell. Biol.*, **26**, 5146–5154.
70. Ghaemmaghami,S., Huh,W.K., Bower,K., Howson,R.W., Belle,A., Dephoure,N., O'Shea,E.K. and Weissman,J.S. (2003) Global analysis of protein expression in yeast. *Nature*, **425**, 737–741.
71. Moore,T., Zhang,Y., Fenley,M.O. and Li,H. (2004) Molecular basis of box C/D RNA-protein interactions; cocrystal structure of archaeal L7Ae and a box C/D RNA. *Structure*, **12**, 807–818.
72. Dobbyn,H.C., McEwan,P.A., Krause,A., Novak-Frazer,L., Bella,J. and O'Keefe,R.T. (2007) Analysis of pre-mRNA and pre-rRNA processing factor Snu13p structure and mutants. *Biochem. Biophys. Res. Commun.*, **360**, 857–862.
73. Lafontaine,D.L. and Tollervey,D. (1999) Nop58p is a common component of the box C+D snoRNPs that is required for snoRNA stability. *RNA*, **5**, 455–467.
74. Kufel,J., Allmang,C., Verdone,L., Beggs,J. and Tollervey,D. (2003) A complex pathway for 3′ processing of the yeast U3 snoRNA. *Nucleic Acids Res.*, **31**, 6788–6797.
75. Goldfeder,M.B. and Oliveira,C.C. (2008) Cwc24p, a novel Saccharomyces cerevisiae nuclear ring finger protein, affects pre-snoRNA U3 splicing. *J. Biol. Chem.*, **283**, 2644–2653.
76. Verheggen,C., Lafontaine,D.L., Samarsky,D., Mouaikel,J., Blanchard,J.M., Bordonne,R. and Bertrand,E. (2002) Mammalian and yeast U3 snoRNPs are matured in specific and related nuclear compartments. *EMBO J.*, **21**, 2736–2745.
77. Pradet-Balade,B., Girard,C., Boulon,S., Paul,C., Azzag,K., Bordonne,R., Bertrand,E. and Verheggen,C. (2011) CRM1 controls the composition of nucleoplasmic pre-snoRNA complexes to licence them for nucleolar transport. *EMBO J.*, **30**, 2205–2218.
78. Gerczei,T. and Correll,C.C. (2004) Imp3p and Imp4p mediate formation of essential U3-precursor rRNA (pre-rRNA) duplexes, possibly to recruit the small subunit processome to the pre-rRNA. *Proc. Natl. Acad. Sci. U.S.A.*, **101**, 15301–15306.
79. Gerczei,T., Shah,B.N., Manzo,A.J., Walter,N.G. and Correll,C.C. (2009) RNA chaperones stimulate formation and yield of the U3 snoRNA-Pre-rRNA duplexes needed for eukaryotic ribosome biogenesis. *J. Mol. Biol.*, **390**, 991–1006.
80. Wormsley,S., Samarsky,D.A., Fournier,M.J. and Baserga,S.J. (2001) An unexpected, conserved element of the U3 snoRNA is required for Mpp10p association. *RNA*, **7**, 904–919.
81. Xue,S., Wang,R., Yang,F., Terns,R.M., Terns,M.P., Zhang,X., Maxwell,E.S. and Li,H. (2010) Structural basis for substrate placement by an archaeal box C/D ribonucleoprotein particle. *Mol. Cell*, **39**, 939–949.
82. Lin,J., Lai,S., Jia,R., Xu,A., Zhang,L., Lu,J. and Ye,K. (2011) Structural basis for site-specific ribose methylation by box C/D RNA protein complexes. *Nature*, **469**, 559–563.
83. Puchta,O., Cseke,B., Czaja,H., Tollervey,D., Sanguinetti,G. and Kudla,G. (2016) Network of epistatic interactions within a yeast snoRNA. *Science*, **352**, 840–844.
84. Ballarino,M., Morlando,M., Pagano,F., Fatica,A. and Bozzoni,I. (2005) The cotranscriptional assembly of snoRNPs controls the biosynthesis of H/ACA snoRNAs in Saccharomyces cerevisiae. *Mol. Cell. Biol.*, **25**, 5396–5403.
85. Grozdanov,P.N., Roy,S., Kittur,N. and Meier,U.T. (2009) SHQ1 is required prior to NAF1 for assembly of H/ACA small nucleolar and telomerase RNPs. *RNA*, **15**, 1188–1197.
86. Yang,P.K., Hoareau,C., Froment,C., Monsarrat,B., Henry,Y. and Chanfreau,G. (2005) Cotranscriptional recruitment of the pseudouridylsynthetase Cbf5p and of the RNA binding protein Naf1p during H/ACA snoRNP assembly. *Mol. Cell. Biol.*, **25**, 3295–3304.